Chemical Geology 549 (2020) 119700

Contents lists available at ScienceDirect

Chemical Geology

journal homepage: www.elsevier.com/locate/chemgeo

Multicomponent diffusion in a basaltic melt: Temperature dependence

Chenghuan Guo (郭城桓), Youxue Zhang (张有学)*

Department of Earth and Environmental Sciences, The University of Michigan, Ann Arbor, MI 48109-1005, USA

ARTICLE INFO

Editor: Donald Dingwell

Keywords:
Multicomponent diffusion matrix
Effective binary diffusivity
Interdiffusivity
Kinetics
Diffusion eigenvectors
Arrhenian eigenvalues
Uphill diffusion
Nearly degenerate eigenvalues
Bushveld

ABSTRACT

Eighteen successful diffusion couple experiments in 8-component SiO_2–TiO_2–Al_2O_3–FeO–MgO–CaO–Na_2O–K_2O basaltic melts were conducted at 1260 °C and 0.5 GPa and at 1500 °C and 1.0 GPa. These experiments are combined with previous data at 1350 °C and 1.0 GPa (Guo and Zhang, 2018) to study the temperature dependence of multicomponent diffusion in basaltic melts. Effective binary diffusion coefficients of components with monotonic diffusion profiles were extracted and show a strong dependence on their counter-diffusing component even though the average (or interface) compositions are the same. The diffusion matrix at 1260 °C was obtained by simultaneously fitting diffusion profiles of all diffusion couple experiments as well as appropriate data from the literature. All features of concentration profiles in both diffusion couples and mineral dissolution are well reproduced by this new diffusion matrix. At 1500 °C, only diffusion couple experiments are used to obtain the diffusion matrix. Eigenvectors of the diffusion matrix are used to discuss the diffusion (exchange) mechanism, and eigenvalues characterize the diffusion rate. Diffusion mechanisms at both 1260 and 1500 °C are inferred from eigenvectors of diffusion matrices and compared with those at 1350 °C reported in Guo and Zhang (2018). There is indication that diffusion eigenvectors in basaltic melts do not depend much on temperature, but complexity is present for some eigenvectors. The two slowest eigenvectors involve the exchange of SiO_2 and/or Al_2O_3 with nonalkalis. The third slowest eigenvector is due to the exchange of divalent oxides with other oxides. The fastest eigenvector is due to the exchange of Na_2O with other oxide components. Some eigenvalues differ from each other by < 1/3, and their eigenvectors are less well defined. We define small difference in eigenvalues as near degeneracy. In strict mathematical degeneracy when two eigenvalues are identical, eigenvectors are not uniquely defined because any linear combination of two eigenvectors is also an eigenvector. In the case of near degeneracy, more constraints either in terms of higher data quality or more experiments are needed to resolve the eigenvectors. We made a trial effort to generate a set of average eigenvectors, which are assumed to be constant as temperature varies. The corresponding eigenvalues are roughly Arrhenian. Thus, the temperature-dependent diffusion matrix can be roughly predicted. The method is applied to predict experimental diffusion profiles in basaltic melts during olivine and anorthite dissolution at ~1400 °C with preliminary success. We further applied our diffusion matrix to investigate multicomponent diffusion during magma mixing in the Bushveld Complex and found such diffusion may result in an increased likelihood of sulfide and Fe—Ti oxide mineralization.

1. Introduction

Natural basaltic melts consist of at least eight major components (e.g. SiO_2, TiO_2, Al_2O_3, FeO, MgO, CaO, Na_2O and K_2O). Therefore, diffusion in such melts is always multicomponent in nature, which must be addressed to predict mass transport in magmatic systems, including mixing and contamination (Sato, 1975; Watson, 1982; Koyaguchi, 1985, 1989; Oldenburg et al., 1989), double-diffusive convection (Turner, 1985; Liang et al., 1996; Richter et al., 1998), and mineral growth or dissolution in magmas (Watson, 1982; Zhang et al., 1989).

In the past, diffusion in natural silicate melts is often treated using the effective binary diffusion (EBD) model (e.g., Cooper, 1968), in which the diffusive flux of a component is assumed to be proportional to the concentration gradient of the component itself and unaffected by the concentration gradients of other components. The method is useful in treating the diffusion of components whose concentration gradient is the largest (e.g., Watson, 1982; Zhang et al., 1989; Chen and Zhang, 2008, 2009), but cannot be used to treat the diffusion of components that show uphill diffusion, which occurs often (e.g., Watson, 1982; Zhang et al., 1989; Zhang, 1993). In addition, the effective binary diffusion coefficient of a given component in a single melt composition at a given temperature and pressure can still vary significantly due to different concentration gradients (Cooper, 1968; Guo and Zhang, 2016, 2018). Moreover, the coordinated motion of components in silicate

* Corresponding author.
E-mail address: youxue@umich.edu (Y. Zhang).

https://doi.org/10.1016/j.chemgeo.2020.119700
Received 8 September 2019; Received in revised form 14 May 2020; Accepted 28 May 2020
Available online 02 June 2020

Table 1
Starting glass compositions (in wt%).

	SiO_2^*	TiO_2	Al_2O_3	FeO_t	MgO	CaO	Na_2O	K_2O
Base Comp	51.00	2.00	14.00	11.50	6.50	10.50	3.00	1.50
JDF Basalts	50.98	1.97	13.81	12.24	7.15	10.91	2.77	0.17
Haplobasalts	50.00	1.50	15.00	0.00	10	19.00	3.00	1.50
BS1	51.81(19)	0.51(02)	14.10(09)	11.67(13)	6.66(04)	10.68(04)	3.07(04)	1.49(02)
BS2	49.47(22)	3.44(06)	14.17(07)	11.15(11)	6.62(06)	10.63(05)	3.05(06)	1.47(03)
BS3	51.85(25)	1.93(06)	12.70(10)	11.67(14)	6.69(06)	10.72(05)	2.98(05)	1.46(02)
BS4	49.31(23)	1.96(05)	15.77(09)	11.18(13)	6.80(05)	10.60(08)	2.98(04)	1.41(02)
BS5	52.19(22)	1.97(03)	14.06(13)	9.88(10)	6.66(05)	10.63(05)	3.06(04)	1.54(03)
BS6	49.19(27)	1.97(03)	14.35(16)	12.65(11)	6.78(07)	10.57(07)	2.99(05)	1.49(01)
BS7	52.00(17)	1.93(05)	14.32(07)	11.48(10)	5.27(04)	10.62(04)	2.98(03)	1.40(02)
BS8	49.29(14)	1.98(03)	14.31(08)	11.27(09)	8.13(08)	10.53(06)	2.98(02)	1.53(02)
BS9	51.59(20)	1.95(06)	14.44(13)	11.34(15)	6.61(05)	9.25(04)	3.23(06)	1.60(02)
BS10	49.18(21)	2.00(04)	14.10(08)	11.39(11)	6.68(06)	12.04(06)	3.02(04)	1.58(03)
BS11	52.21 (16)	2.01(05)	14.14(08)	11.19(08)	6.81(06)	10.59(05)	1.54(03)	1.53(02)
BS12	49.43(16)	2.01(04)	14.08(11)	11.22(06)	6.72(07)	10.54(05)	4.48(04)	1.52(02)
BS13	52.54(19)	1.98(05)	13.88(10)	11.43(11)	6.67(07)	10.51(05)	2.95(07)	0.04(01)
BS14	49.31(24)	2.02(03)	13.98(10)	11.52(10)	6.60(07)	10.57(05)	2.98(05)	3.04(04)
BS17	50.55(21)	1.96(05)	14.25(10)	11.31(08)	8.14(09)	10.80(05)	2.95(03)	0.04(01)
BS18	50.50(14)	1.94(05)	14.15(09)	11.56(07)	5.29(07)	10.65(04)	2.92(04)	3.00(03)
BS19	50.58(19)	2.02(03)	15.82(09)	11.23(09)	6.68(07)	9.14(06)	3.03(03)	1.49(02)
BS20	50.66(17)	1.96(05)	12.78(09)	11.50(12)	6.68(05)	11.98(05)	2.91(05)	1.51(03)

Note: 1. BS stands for basalt. 2. The values in parentheses are 1σ errors on the last digit.
3. SiO_2^* is define as $SiO_2^* = SiO_2 - (total - 100)$, so that the new "total" is 100% (Guo and Zhang, 2016, 2018). The unnormalized composition at each point can be found in the Supplementary table.

Table 2
Summary of experimental conditions.

Exp#	T	P	Duration	Couples
	°C	GPa	s	
BS1&2C	1260	0.5	1826	Si–Ti
BS3&4C	1260	0.5	1810	Si–Al
BS5&6C	1260	0.5	1326	Si–Fe
BS7&8C	1260	0.5	1269	Si–Mg
BS9&10C	1260	0.5	951	Si–Ca
BS11&12C	1260	0.5	580	Si–Na
BS13&14C	1260	0.5	740	Si–K
BS17&18C	1260	0.5	577	Mg–K
BS19&20C	1260	0.5	600	Al–Ca
BS1&2B	1500	1.0	276	Si–Ti
BS3&4B	1500	1.0	224	Si–Al
BS5&6B	1500	1.0	248	Si–Fe
BS7&8B	1500	1.0	214	Si–Mg
BS9&10B	1500	1.0	159	Si–Ca
BS11&12B	1500	1.0	157	Si–Na
BS13&14B	1500	1.0	155	Si–K
BS17&18B	1500	1.0	185	Mg–K
BS19&20B	1500	1.0	221	Al–Ca

Note: Durations listed are calculated effective experimental durations (Zhang and Behrens, 2000) at either 1260 °C or 1500 °C using an activation energy of 155 kJ/mol (see text).

melts (e.g., Watson, 1982; Zhang et al., 1989; Macris et al., 2018) must be understood in the context of multicomponent diffusion.

Tremendous efforts have been made in studying multicomponent diffusion in various silicate melts (Varshneya and Cooper, 1972; Sugawara et al., 1977; Oishi et al., 1982; Kress and Ghiorso, 1993, 1995; Chakraborty et al., 1995a,b; Mungall et al., 1998; Liang, 2010; Watkins et al., 2014; Claireaux et al., 2016, 2019; Guo and Zhang, 2016, 2018; Pablo et al., 2017). Most previous studies on multicomponent diffusion were on relatively simple silicate melt systems. Guo and Zhang (2018) first reported a complete diffusion matrix at 1350 °C in 8-component SiO_2–TiO_2–Al_2O_3–FeO–MgO–CaO–Na_2O–K_2O basaltic melts, and applied it to predict olivine, diopside and anorthite dissolution in basaltic melts at the same temperature. For more applications, it is necessary to quantify multicomponent diffusion in natural melts at various temperatures.

In an N-component system, defining $n = N–1$, the diffusion matrix $[D]$ is an n by n square matrix (where [] means a square matrix). The $[D]$ matrix can be decomposed as the product of $[P][\lambda][P^{-1}]$, where matrix $[P]$ is the eigenvector matrix (an n by n square matrix), $[P^{-1}]$ is the inverse matrix of $[P]$, and $[\lambda]$ is the eigenvalue matrix (an n by n diagonal square matrix with each diagonal being an eigenvalue) (Zhang, 2008). The eigenvector matrix is made of n column eigenvectors $\mathbf{v_i}$ that each satisfies the condition that $[D]$ times $\mathbf{v_i}$ is proportional to $\mathbf{v_i}$, with the proportionality being the eigenvalue λ_i. In general, both eigenvectors and eigenvalues of diffusion matrices of silicate melts are expected to depend on temperature, pressure and composition. It has been shown that in some ternary (SiO_2-SrO-K_2O, SiO_2–Al_2O_3-K_2O, SiO_2–Al_2O_3-CaO, SiO_2-B_2O_3-Na_2O) and quaternary (SiO_2–Al_2O_3-MgO-CaO, SiO_2–Al_2O_3–CaO-Na_2O, SiO_2-$NaAlSi_3O_8$-$KAlSi_3O_8$-H_2O) silicate melt systems, the diffusion eigenvectors are not very sensitive to variations in temperature, pressure, and even composition in a given system (Varshneya and Cooper, 1972; Sugawara et al., 1977; Oishi et al., 1982; Chakraborty et al., 1995b; Mungall et al., 1998; Liang and Davis, 2002; Liang, 2010; Pablo et al., 2017; Claireaux et al., 2019), whereas eigenvalues often exhibit an Arrhenian dependence on temperature (but see Pablo et al., 2017 for an exception). If this empirical observation also applies to basaltic melts, it would provide a way to simplify and quantify the temperature dependence of the diffusion matrix.

Here, we expand our earlier study (Guo and Zhang, 2018) to investigate the temperature dependence of the diffusion matrix in the same basaltic melt. To understand how the diffusion matrix depends on temperature, following our previous work on multicomponent diffusion in basaltic melts at 1350 °C (Guo and Zhang, 2018), diffusion couple experiments in the same 8-component basaltic melts at two new temperatures 1260 and 1500 °C were conducted. We fit the experimental data to obtain the diffusion matrix at each temperature. Then, the temperature dependence of diffusion matrices is examined by evaluating the temperature dependence of corresponding eigenvalues and eigenvectors.

2. Experimental and analytical methods

The experimental designs for diffusion couples followed those in Guo and Zhang (2016, 2018). A base composition is chosen to be

Table 3
Effective binary diffusion coefficients (in $\mu m^2/s$).

Exp#	$D(SiO_2)$	$D(TiO_2)$	$D(Al_2O_3)$	$D(FeO_t)$	$D(MgO)$	$D(CaO)$	$D(Na_2O)$	$D(K_2O)$
BS1&2C	1.4 ± 0.2	2.4 ± 0.1						
BS3&4C	1.7 ± 0.2		1.8 ± 0.1					
BS5&6C	3.5 ± 0.5			10.3 ± 0.7				
BS7&8C	1.3 ± 0.3				7.2 ± 0.3			
BS9&10C	1.6 ± 0.4					10.1 ± 0.5		
BS11&12C	2.6 ± 0.6						208 ± 7	
BS13&14C	13.5 ± 1.8							23.9 ± 0.7
BS17&18C					11.7 ± 0.6			20.3 ± 0.5
BS19&20C			2.9 ± 0.2			15.8 ± 0.7		
BS1&2B	6.6 ± 1.6	16.5 ± 0.8						
BS3&4B	11.0 ± 2.2		16.9 ± 1.2					
BS5&6B	26.9 ± 3.7			49.7 ± 3.5				
BS7&8B	21.7 ± 2.6				69.2 ± 2.7			
BS9&10B	27.8 ± 5.4					102 ± 4		
BS11&12B	38.7 ± 5.6						516 ± 16	
BS13&14B	88 ± 11							135 ± 3
BS17&18B					69.1 ± 3.5			89.3 ± 1.6
BS19&20B			25.9 ± 1.6			97 ± 3		

Note: The first nine experiments (Exp# ends with C) were at 1260 °C and 0.5 GPa. The last nine experiments (Exp# ends with B) were at 1500 °C and 1.0 GPa.

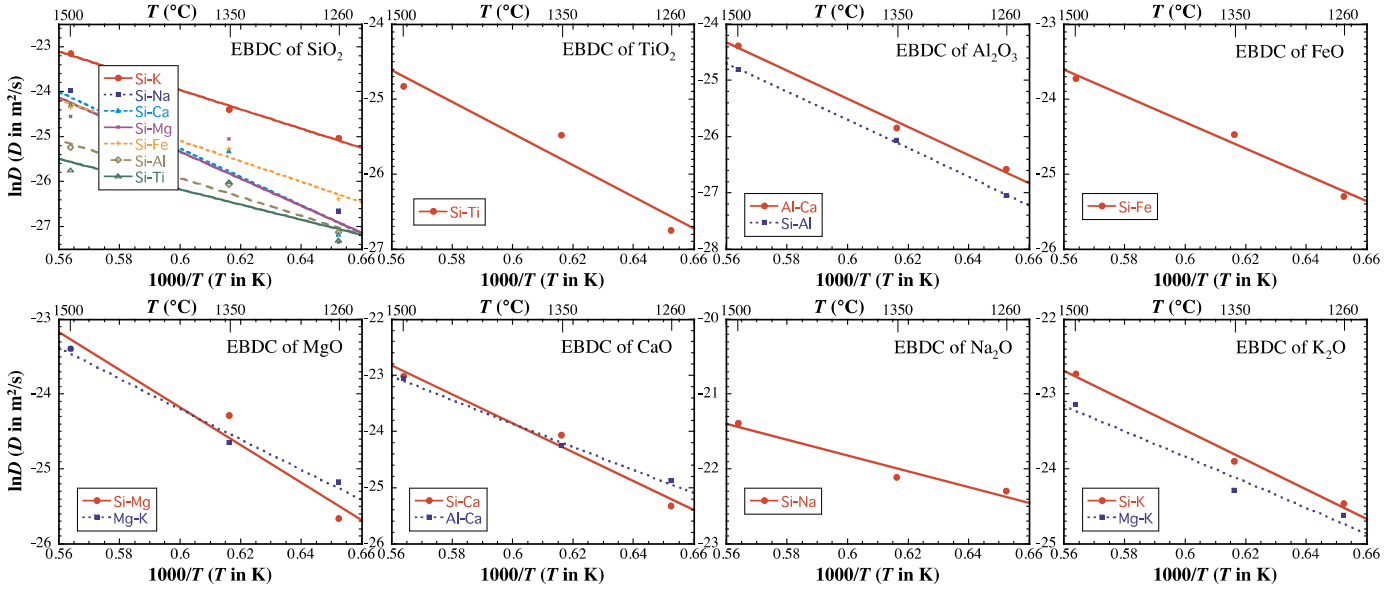

Fig. 1. Temperature dependence of EBDC of each component. Each panel in the figure represents one component, and different symbols indicate EBDC obtained from different diffusion couples. Temperatures are 1500, 1350 and 1260 °C. Data are from this work (1500 and 1260 °C) and Guo and Zhang (2018).

similar to a mid-ocean ridge basalt from Juan De Fuca (JDF) Ridge (Dixon et al., 1988; Zhang and Stolper, 1991), except for K_2O, whose concentration is increased to 1.5 wt% so as to examine the effect of K_2O on the diffusion of other oxides. This base composition, as well as the starting compositions for the diffusion couples are the same as that in Guo and Zhang (2018) who investigated multicomponent diffusion in this melt at 1350 °C and 1 GPa. The goal of this study is to determine the multicomponent diffusion matrix at 1500 °C and 1260 °C in this base composition using diffusion couple experiments so as to investigate the temperature dependence of the diffusion matrix. The basic strategy is also the same as that in Guo and Zhang (2018): Nine diffusion couple experiments were carried out. Each diffusion couple is made of two halves, one half deviates from the base composition by +1.5 wt% in one oxide component and −1.5 wt% in another oxide component, and the other half deviates in the opposite and complimentary way. For experiments at each temperature, the first 7 experiments have initial concentration differences between SiO_2 and another component i, where i = TiO_2, Al_2O_3, FeO, MgO, CaO, Na_2O and K_2O, which are the minimum required to obtain the 7 × 7 diffusion matrix in an 8-component system (Trial and Spera, 1994), unless the analytical data precision is much higher than that of a regular electron microprobe (Liang, 2010). The additional 2 experiments are for further constraints.

Eighteen different starting glasses were made for nine diffusion couple experiments in Guo and Zhang (2018) and these glasses are used in this study. For convenience, the base composition, and the starting compositions of diffusion couples are listed here in Table 1. There may be small differences in the listed compositions in Table 1 here compared to those in Guo and Zhang (2018) due to new analyses of the samples. For comparison, the compositions of the JDF basalt and a haplobasalt base composition that was used in the multicomponent diffusion study by Guo and Zhang (2016) are also listed in Table 1.

The diffusion couple experiments were conducted in a 12.7-mm piston cylinder apparatus and followed the procedure described in Guo and Zhang (2018) but at different temperatures (Table 2). Even though the pressure for the 1350 °C experiments (Guo and Zhang, 2018) and the 1500 °C experiments (this study) is 1 GPa, the pressure for the lowest temperature experiments at ~1260 °C was chosen to be 0.5 GPa

Table 4
Diffusion matrix $D_{1260°C}^{couples}$($\mu m^2/s$), obtained by fitting the 9 diffusion couple experiments at ~1260 °C, and eigenvalues ($\mu m^2/s$) and eigenvectors.

$D_{1260°C}^{couples}$	TiO_2	Al_2O_3	FeO	MgO	CaO	Na_2O	K_2O
TiO_2	2.47(7)	–0.11(6)	–1.12(18)	–0.30(21)	–0.50(29)	–1.79(89)	–1.43(34)
Al_2O_3	–0.01(21)	2.01(11)	–2.62(40)	–0.16(47)	–3.39(63)	–8.77(238)	–6.30(75)
FeO	–7.24(70)	0.18(53)	5.02(66)	–30.4(11)	–40.1(12)	–105(3)	–42.0(13)
MgO	–2.12(31)	0.66(21)	–6.83(33)	5.67(53)	–12.1(6)	–30.3(18)	–13.7(7)
CaO	–2.46(26)	–3.07(18)	–7.20(32)	–9.44(41)	9.04(55)	–26.8 (15)	–0.65(64)
Na_2O	10.5(11)	2.03(69)	20.6(7)	32.5(9)	47.6(11)	186(2)	59.0(11)
K_2O	1.28(13)	0.96(9)	2.38(15)	3.65(20)	5.13(27)	4.22(68)	25.4(4)
Eigenvalues (from small to large)							
	λ_1	λ_2	λ_3	λ_4	λ_5	λ_6	λ_7
	1.764(72)	2.02(10)	3.55(11)	16.39(49)	22.74(72)	26.71(60)	163.7(20)
Eigenvectors							
	v_1	v_2	v_3	v_4	v_5	v_6	v_7
TiO_2	–0.48(10)	–0.37(19)	–0.42(6)	–0.008(15)	–0.04(2)	0.017(15)	–0.005(5)
Al_2O_3	*–0.10(34)*	*0.79(96)*	–0.33(9)	–0.09(3)	–0.09(4)	–0.015(26)	–0.036(18)
FeO	–0.59(9)	–0.37(15)	0.61(5)	0.29(16)	*0.93(89)*	*–0.72(36)*	–0.51(24)
MgO	–0.35(7)	–0.27(12)	0.42(3)	–0.60(12)	–0.19(10)	–0.03(6)	–0.13(6)
CaO	–0.45(3)	–0.11(4)	0.35(2)	0.71(11)	–0.29(20)	0.59(13)	–0.11(5)
Na_2O	0.21(2)	0.11(3)	–0.16(1)	–0.05(2)	–0.019(14)	–0.19(1)	*0.84(54)*
K_2O	0.21	0.07	–0.15	–0.21	0.08	0.31	0.01
Eigenvectors (showing all 8 components)							
	v_1	v_2	v_3	v_4	v_5	v_6	v_7
SiO_2	0.842	0.150	–0.308	–0.050	–0.351	0.043	–0.054
TiO_2	–0.257	–0.367	–0.395	–0.008	–0.042	0.017	–0.005
Al_2O_3	–0.055	0.781	–0.316	–0.095	–0.080	–0.015	–0.035
FeO	–0.317	–0.368	0.579	0.292	0.868	–0.718	–0.508
MgO	–0.190	–0.263	0.399	–0.595	–0.182	–0.034	–0.132
CaO	–0.246	–0.110	0.335	0.710	–0.274	0.591	–0.114
Na_2O	0.112	0.105	–0.152	–0.047	–0.018	–0.191	0.841
K_2O	0.111	0.071	–0.142	–0.207	0.079	0.308	0.009

Note: The values in parentheses are 1σ errors on the last digit. Red color means the error is ≥0.2 for an oxide component in an eigenvector. The eigenvectors showing all 8 components are for easy discussion of dominant exchange mechanisms. The SiO_2 component in each eigenvector is calculated from the 7–component eigenvector, by adding the SiO_2 component so that the summation of all components in the eigenvector is zero. Then each all–component eigenvector is unitarized. To obtain the independent 7-component eigenvectors, one first removes the SiO_2 row and then unitarize each column vector.

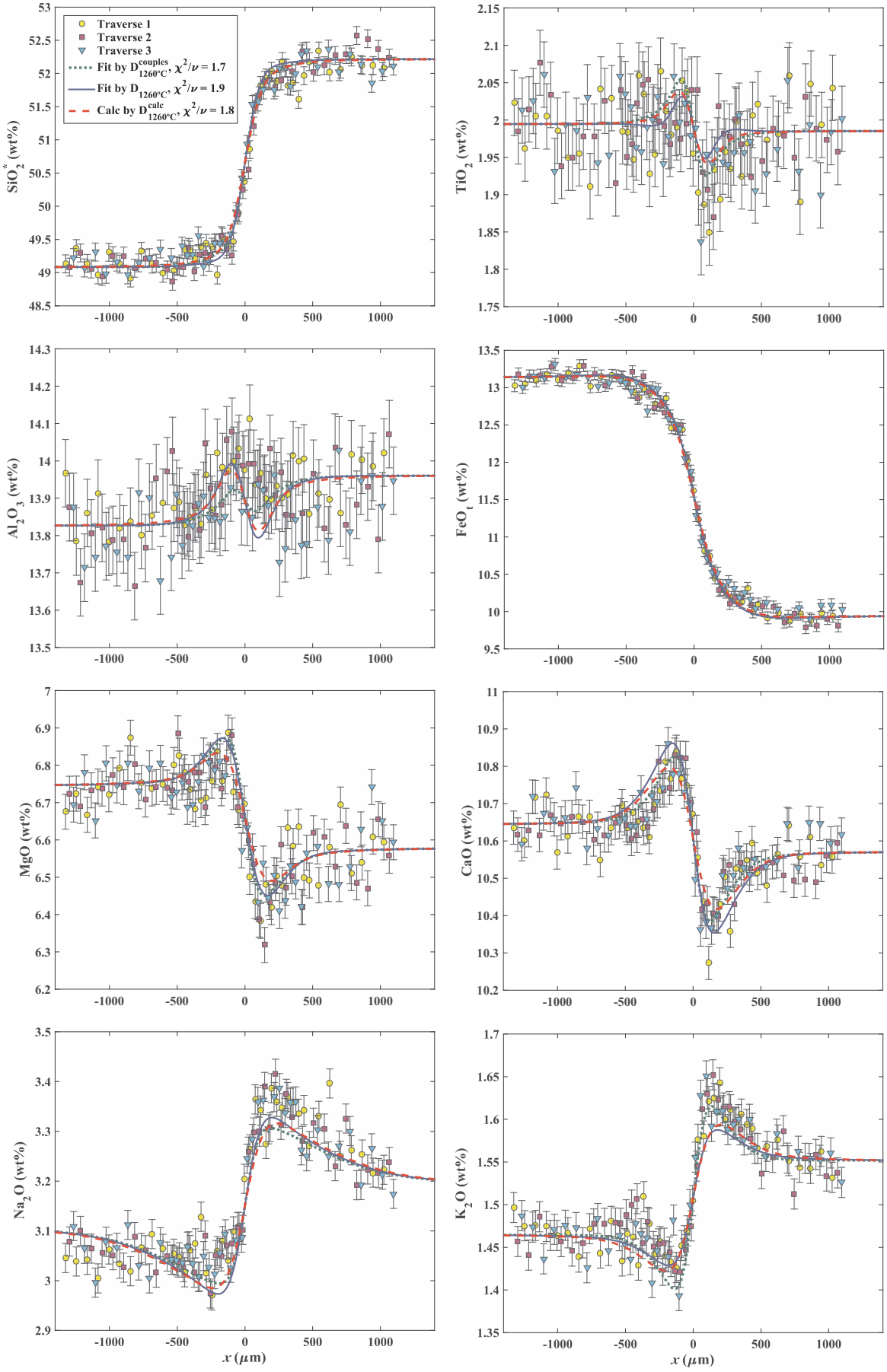

(caption on next page)

Fig. 2. Data of diffusion profiles of BS5&6C with fits and prediction. All the points are measured data. Different symbols indicate different traverses. The error bars are ± 1σ errors. The short-dashed green curves are fit profiles for obtaining the diffusion matrix $D_{1260^oC}^{couples}$ (Table 4). The solid blue curves are fit profiles for obtaining the diffusion matrix D_{1260^oC} (Table 6). The long-dashed red curves are predicted profiles using the calculated diffusion matrix by Eq. (4) and Table 8 at 1260 °C. Data of diffusion profiles of other diffusion couple experiments with fits at 1260 °C are shown in the supplementary file. χ^2/ν (MSWD) is calculated and shown for each type of fits and prediction. (For interpretation of the references to color in this figure legend, the reader is referred to the web version of this article.)

because higher pressure would lead to partial crystallization. Literature data show that the variation of diffusion coefficients in JDF melt from 0.5 to 1.4 GPa is within data uncertainty (e.g., Chen and Zhang, 2008, 2009; Zhang et al., 2010; Yu et al., 2016). Hence, we make this compromise of using 0.5 GPa rather than 1.0 GPa so that a temperature of 1260 °C (lower than 1350 °C by 90 °C) can be used to cover a larger total temperature range for the assessment of the temperature effect of the diffusion matrix. In addition, magmatic temperatures are often between 1200 and 1350 °C, and a lower-temperature experiment down to 1260 °C would better allow data to be applied to magmatic processes.

During a diffusion experiment, temperature at the top of the graphite capsule was continuously monitored using a type-S thermocouple. Temperature fluctuation is typically ± 1 °C, but temperature uncertainty is larger (probably 10 or even 20 °C) due to imperfect alignment of the interface position with the hotspot position although effort was made to account for the temperature difference between the thermocouple and the diffusion couple interface (Hui et al., 2008). The temperature, pressure and corrected duration of the experiments are listed in Table 2.

After quenching, the experimental charges were prepared and then analyzed by a Cameca SX100 electron microprobe at the University of Michigan, following the same procedure described in Guo and Zhang (2018). Three traverses were measured to obtain diffusion profiles for each diffusion couple experiment. As discussed later, literature data from mineral dissolution experiments by Chen and Zhang (2008, 2009) and Yu et al. (2016) will also be used to better constrain diffusion matrices.

3. Experimental results and effective binary diffusion coefficients

Eighteen successful diffusion couple experiments were carried out, of which 9 experiments are at ~1260 °C and 0.5 GPa and the other 9 experiments are at ~1500 °C and 1 GPa (Table 2). The experiment ID (Exp# in Tables 2 and 3) indicates the two halves of initial glasses as well as the experimental temperature. For example, BS1&2C indicates that one half is BS1, the other half is BS2, which were melted together at the experimental temperature of 1260 °C for diffusion (the last letter "C" in the Exp# means 1260 °C and "B" means 1500 °C). Quench cracks are observed in 3 out of 18 experiments. Physical interface can be seen by a small dent or misalignment near the contact with the graphite crucible. For crack-present experiments, concentration profiles near cracks are re-connected smoothly by comparing different traverses. All diffusion profiles of microprobe analytical data can be found in the Supplementary files.

Effective experimental durations were calculated by $t_{\text{eff}} = \int e^{-E/(RT)} dt / e^{-E/(RT_{\text{exp}})}$ (Zhang and Behrens, 2000), where T_{exp} for each experiment is listed in Table 2, T is temperature in K and depends on time including heating up and cooling down, and E is the activation energy for diffusion. In the first round of calculating the effective experimental durations for all experiments, an activation energy of 230 kJ/mol (averaging activation energy for MgO diffusion in Chen and Zhang, 2008, 2009) is used. The effective durations are used in obtaining the diffusion matrices at 1260 °C and 1500 °C. Then each of the seven eigenvalues at 1260 °C and 1500 °C (this study) and 1350 °C (Guo and Zhang, 2018) is plotted in an Arrhenius diagram to obtain the activation energy E. The average of the seven E's is 155 kJ/mol. This value of E (155 kJ/mol) is used to recalculate the effective durations of all experiments, which are then used to obtain effective binary diffusivities as well as the diffusion coefficient matrices. The duration correction (i.e., difference between t_{eff} and experimental duration at the peak temperature) is small, < 10% of the total duration. That is, even though the correction is imperfect, the error in D introduced by the correction is < 10% relative.

The electron microprobe data with distance together with the experimental duration are the key data used in fitting to determine effective binary diffusion coefficients and multicomponent diffusion matrices. Before fitting, the preliminary data were processed following the same procedure in Guo and Zhang (2018). First, $SiO_2^* = SiO_2 - (\text{total} - 100)$ is used as replacement for SiO_2 in fitting because SiO_2^* concentration profile shows less scatter than SiO_2. Second, boundary conditions and 1σ errors needed for multicomponent diffusion fitting were determined by taking the average and standard deviation of data points in the far-fields in diffusion profiles.

Effective binary diffusion coefficients (EBDC) were obtained for the two oxide components with initial concentration difference of ~3 wt%. Most of these profiles show "normal" behavior (no uphill diffusion) and are fit (Figs. S1–S6) by the following equation:

$$w = \frac{w_{-\infty} + w_{+\infty}}{2} + \frac{w_{+\infty} - w_{-\infty}}{2} \cdot \text{erf}\left(\frac{x - x_0}{2\sqrt{Dt}}\right), \quad (1)$$

where w is the concentration (in wt%) of the oxide, $w_{-\infty}$ and $w_{+\infty}$ are the left and right far-field concentrations, x is the position (often in μm), x_0 is the interface position, D is the effective binary diffusion coefficient (often in $\mu m^2/s$), and t is the corrected experimental duration. Eq. (1) is the solution for a constant effective binary diffusivity D. If the equation fits the data within uncertainty, it justifies the constant D assumption. D and x_0 are the two parameters to be determined from the fit. The x_0 values of the best-resolved profile is used to define new coordination $x_{\text{new}} = x - x_0$ for fitting multicomponent diffusion matrix such that the new interface position is at $x_{\text{new}} = 0$.

The fits are shown in the supplementary files (Figs. S1–S6): For oxides other than SiO_2, the fits are excellent and r^2 ranges from 0.9923 to 0.9995. For SiO_2, there is more scatter due to larger measurement uncertainty (1σ ~ 0.2 wt%), and r^2 ranges from 0.967 to 0.986. Some fits show small systematic misfit, attributed to the effect of multicomponent diffusion. The EBDC values are reported in Table 3. Note that even though each diffusion couple is set up as roughly interdiffusion between two oxides, the EBDC of the two oxides are not the same. For example, for Exp BS9&10C, $D_{SiO2} = 1.59 \pm 0.34$ $\mu m^2/s$ (1 $\mu m^2/s = 10^{-12}$ m^2/s), whereas $D_{CaO} = 10.1 \pm 0.5$ $\mu m^2/s$. (The diffusing species are not known, and the subscript for an effective binary diffusivity indicates the diffusing oxide; that is, D_{SiO2} and D_{CaO} were obtained by fitting the SiO_2 and CaO concentration profiles respectively using Eq. (1)) The difference reflects the influence of other components during diffusion. Furthermore, our data show that EBDC of a given component in this multicomponent basalt system with a single bulk composition (which is the base composition) is strongly dependent on its counter-diffusing component. That is, our data experimentally

Table 5
Diffusion matrix $D_{1500°C}^{couples}$ ($\mu m^2/s$), obtained by fitting the 9 diffusion couple experiments at ~1500 °C, and eigenvalues and eigenvectors.

$D_{1500°C}^{couples}$	TiO_2	Al_2O_3	FeO	MgO	CaO	Na_2O	K_2O
TiO_2	16.8(9)	–0.82(44)	–5.34(98)	0.34(99)	–6.51(133)	–7.87(348)	–4.97(140)
Al_2O_3	–2.89(144)	14.16(97)	–11.5(23)	–13.7(24)	–39.3(29)	–81.7(82)	–58.0(36)
FeO	–28.1(24)	–13.2(21)	54.7(32)	–90.0(33)	–68.3(41)	–114.7(96)	–103.6(42)
MgO	–5.42(161)	3.26(124)	–29.3(23)	70.7(25)	–43.7(26)	–84.8(65)	–26.6(30)
CaO	–4.10(159)	–5.02(145)	–20.6(21)	–20.2(22)	106.8(26)	–14.1(53)	54.7(26)
Na_2O	35.7(40)	25.7(25)	76.2(41)	82.5(22)	130.5(47)	551(17)	178(5)
K_2O	7.07(80)	4.42(51)	11.2(10)	23.8(9)	22.0(11)	21.7(22)	130.9(17)
Eigenvalues (diagonal matrix, from small to large)							
	λ_1	λ_2	λ_3	λ_4	λ_5	λ_6	λ_7
	13.75(73)	17.68(88)	32.0(11)	98.6(28)	116.9(38)	145.0(33)	520.7(168)
Eigenvectors							
	v_1	v_2	v_3	v_4	v_5	v_6	v_7
TiO_2	–0.69(9)	–0.17(15)	–0.24(3)	–0.034(19)	–0.056(68)	–0.015(12)	–0.013(7)
Al_2O_3	0.31(27)	0.97(223)	–0.14(8)	–0.013(30)	–0.09(11)	–0.145(27)	–0.148(25)
FeO	–0.52(4)	–0.12(7)	0.70(6)	0.84(28)	0.55(76)	–0.46(11)	–0.204(35)
MgO	–0.24(4)	–0.15(15)	0.43(3)	–0.30(13)	–0.61(91)	–0.093(85)	–0.169(31)
CaO	–0.24(2)	–0.03(2)	0.41(2)	–0.37(10)	0.54(81)	0.79(16)	–0.008(13)
Na_2O	0.15(1)	0.004(20)	–0.18(1)	–0.071(28)	–0.15(17)	–0.254(25)	0.95(26)
K_2O	0.146	0.020	–0.212	0.241	0.032	0.265	0.035
Eigenvectors (showing all 8 components)							
	v_1	v_2	v_3	v_4	v_5	v_6	v_7
SiO_2	0.736	–0.467	–0.611	–0.297	–0.218	–0.088	–0.408
TiO_2	–0.469	–0.148	–0.191	–0.033	–0.055	–0.015	–0.012
Al_2O_3	0.207	0.855	–0.110	0.012	–0.085	–0.145	–0.135
FeO	–0.349	–0.107	0.554	0.802	0.536	–0.458	–0.186
MgO	–0.162	–0.131	0.343	–0.291	–0.595	–0.093	–0.154
CaO	–0.164	–0.023	0.324	–0.356	0.528	0.787	–0.007
Na_2O	0.103	0.004	–0.141	–0.068	–0.143	–0.253	0.870
K_2O	0.099	0.018	–0.168	0.230	0.031	0.264	0.032

See notes in Table 4.

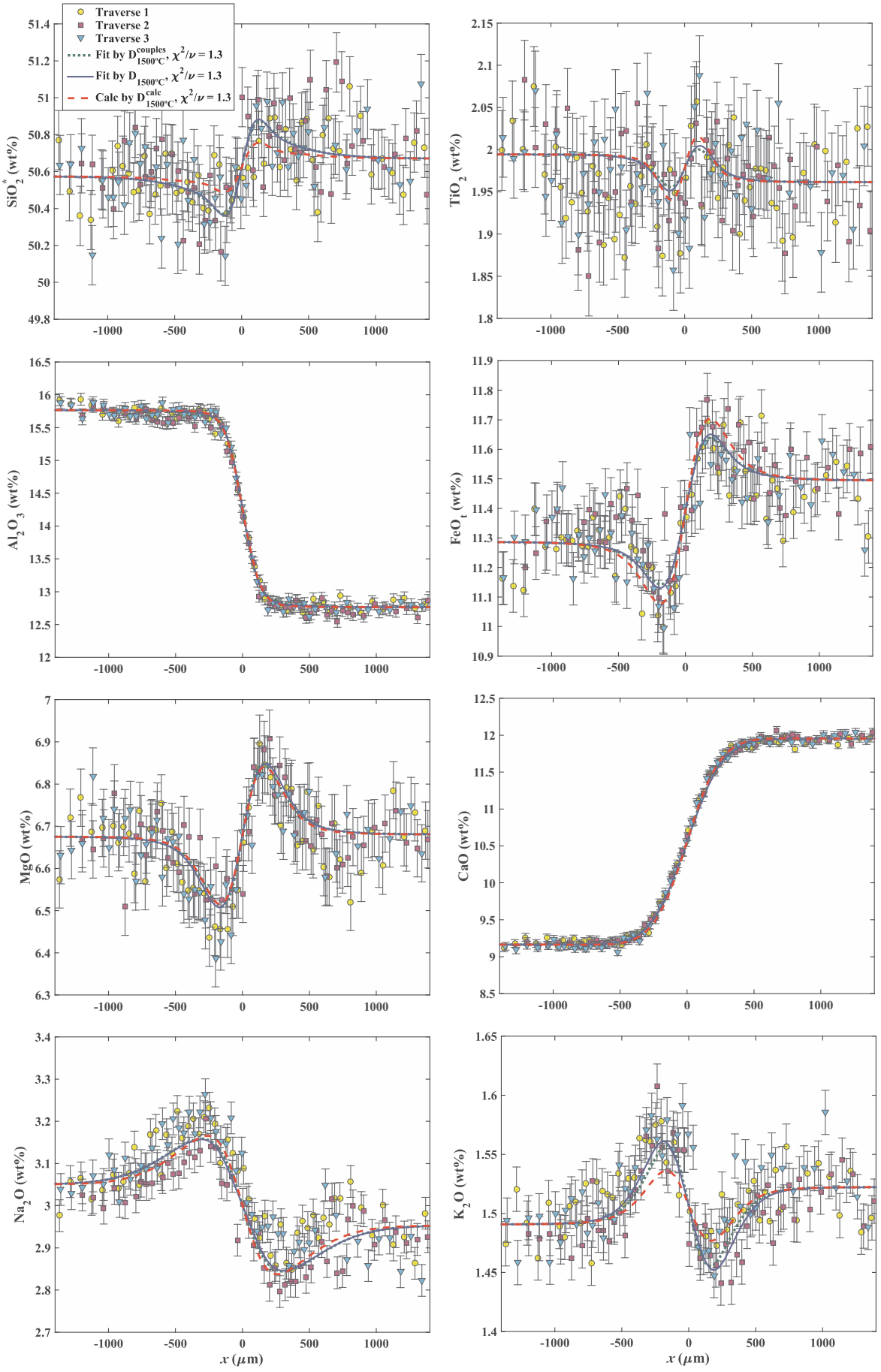

(caption on next page)

Fig. 3. Data of diffusion profiles of BS19&20B with fits and prediction. All the points are measured data. Different symbols indicate different traverses. The error bars are ± 1σ errors. The short-dashed green curves are fit profiles for obtaining the diffusion matrix $D_{1500°C}^{couples}$ (Table 5). The solid blue curves are trial fit profiles for obtaining $D_{1500°C}$. The long-dashed red curves are predicted profiles using the calculated diffusion matrix by Eq. (4) and Table 8 at 1500 °C. Data of diffusion profiles of other diffusion couple experiments with fits at ~1500 °C are shown in the supplementary file. χ^2/ν (MSWD) is calculated and shown for each type of fits and prediction. (For interpretation of the references to color in this figure legend, the reader is referred to the web version of this article.)

confirm the conclusion in Cooper (1968) and are consistent with Guo and Zhang (2016, 2018). The variation in EBDC is especially significant for SiO_2, partially due to more diffusion couples with concentration differences in SiO_2. At 1260 °C, EBDC of SiO_2 varies by a factor of 10, from 1.4 $\mu m^2/s$ when diffusing against TiO_2 to 13.5 $\mu m^2/s$ when diffusing against K_2O; at 1500 °C, EBDC of SiO_2 varies by a factor of 13.3, from 6.6 $\mu m^2/s$ when diffusing against TiO_2 to 88.0 $\mu m_2/s$ when diffusing against K_2O.

Fig. 1 shows temperature dependence of EBDC of each component, where each panel represents one component and different symbols indicate EBDC's obtained from different diffusion couples. It can be seen that there is a large variation in EBDC at a given temperature due to exchange with different components, but EBDC's for each exchange at different temperatures still roughly follow the Arrhenius relation.

4. Diffusion matrix calculation and discussion

4.1. Fitting diffusion couples to obtain D matrix

All diffusion profiles from all nine diffusion couples at the same temperature were fit simultaneously to obtain the diffusion matrix, by minimizing the following χ^2 using Levenberg-Marquardt-Fletcher method (Fletcher, 1971):

$$\chi^2 = \frac{1}{2}\sum_{k=1}^{Nd}\sum_{j=1}^{Np_k}\sum_{i=1}^{Nc}\left(\frac{w_{ijk}^{meas} - w_{ijk}^{calc}}{\sigma_{ik}}\right)^2, \quad (2)$$

where Nd is the number of experiments, Np_k is the number of measured data points in diffusion couple experiment k, Nc is the number of components ($Nc = 8$), w_{ijk}^{meas} and w_{ijk}^{calc} are respectively the measured and calculated concentrations of component i at position j in experiment k, and σ_{ik} is the 1σ error of w_{ijk}^{meas}. Each w_{ijk}^{calc} was calculated from the analytical solution to the multicomponent diffusion problem given by Eq. (A5) in Appendix A1 of Guo and Zhang (2016):

$$w_{ij} = \frac{w_{-\infty,ik} + w_{+\infty,ik}}{2} + [P][\Lambda][P^{-1}]\cdot\frac{w_{+\infty,ik} - w_{-\infty,ik}}{2}, \quad (3)$$

where $[\Lambda]$ is a diagonal matrix with diagonal elements $\Lambda_{mm} = \mathrm{erf}(x_{jk}/\sqrt{4\lambda_m t_k})$ and $\Lambda_{mn} = 0$ when $m \neq n$, λ_m's are the eigenvalues of $[D]$, t_k is the experimental duration of experiment k, and columns of $[P]$ are the eigenvectors of $[D]$.

4.1.1. Diffusion matrix $D_{1260°C}^{couples}$

The diffusion matrix obtained by fitting 9 diffusion couple experiments at 1260 °C is denoted as $D_{1260°C}^{couples}$ and is shown in Table 4. The error of the diffusion matrix is estimated by error propagation in the fitting program (Clifford, 1973) hereafter. The fit curves for experiment BS5&6C are shown by the green short dashed curves in Fig. 2. Fits of data by $D_{1260°C}^{couples}$ for all 9 diffusion couple experiments at 1260 °C are shown by green short dashed curves in Figs. S7–S15 in the Supplementary file. It can be seen that all features in concentration profiles are well reproduced by the obtained diffusion matrix $D_{1260°C}^{couples}$. The goodness of the fit of the eight profiles in an experiment by $D_{1260°C}^{couples}$ is assessed by the reduced chi-squares (also known as mean square weighted deviation, MSWD) shown in each figure. An MSWD value of about 1 means an excellent fit within data uncertainty.

Eigenvalues and eigenvectors of the diffusion matrix $D_{1260°C}^{couples}$ are shown in Table 4. Errors for the eigenvalues and eigenvectors are also estimated from the fitting program and reported in Table 4. Because the diffusion matrix contains $7 \times 7 = 49$ parameters, whereas eigenvalues and eigenvectors contain 56 parameters, the errors of only 49 parameters can be constrained. The errors for eigenvalues and the first six components in every 7-component eigenvector are calculated based on error propagation. While the eigenvector indicates exchanging mechanism, its eigenvalue indicates diffusivity (rate) along an associated direction. The results in Table 4 show that eigenvalues have small relative errors ($\leq$5%). However, some eigenvectors are not well constrained with major errors (red and italicized in Table 4). Therefore, it is necessary to improve our experimental design in the future, to be discussed in a later Section 5.2. Based on eigenvectors listed in Table 4 showing all 8 components, diffusion mechanisms may be inferred. Eigenvector v_1 (smallest eigenvalue) is largely due to the exchange of SiO_2 with other components; v_2 (second smallest) is largely due to the exchange of Al_2O_3 with other components; v_3 is due to the exchange of FeO + MgO + CaO with all other components; v_4 is due to the exchange of CaO + FeO with all other components; v_5 is largely due to the exchange of FeO with all other components; v_6 (second largest) is due to the exchange of CaO + K_2O with all other components; and v_7 (largest eigenvalue) is due to the exchange of Na_2O with all other components. Note that v_3 seems to be best constrained (smallest errors in all components) rather than the eigenvector associated with the largest eigenvalue or that with the smallest eigenvalue. Also note that K_2O is not a dominant component in any eigenvector (in eigenvectors showing all 8 components, the component K_2O is much smaller than 0.5 in any eigenvector).

4.1.2. Diffusion matrix $D_{1500°C}^{couples}$

The obtained diffusion matrix using 9 diffusion couple experiments at 1500 °C is denoted as $D_{1500°C}^{couples}$ and shown in Table 5, including the eigenvalues and eigenvectors. The fit curves for experiment BS19&20B are shown by the green short-dash curves in Fig. 3. Fits by $D_{1500°C}^{couples}$ for all 9 diffusion couple experiments at 1500 °C are shown by green short-dashed curves in Figs. S16–S24 in the Supplementary file. It can be seen that all features in diffusion profiles are well reproduces by this diffusion matrix $D_{1500°C}^{couples}$. The goodness of the fit of the eight profiles in an experiment by $D_{1500°C}^{couples}$ is assessed by the reduced chi-squares shown in each figure.

The eigenvectors at 1500 °C are similar to those at 1260 °C, but with small differences. For example, v_4 at 1500 °C is due to the exchange of FeO + K_2O with all other components, but at 1260 °C it is due to the exchange of CaO + FeO with all other components; v_5 at 1500 °C is largely due to the exchange between FeO + CaO and other oxides, but at 1260 °C it is largely due to the exchange of FeO with all other components. The difference between v_5 at 1500 °C and v_5 at 1260 °C may be attributed to large errors in the FeO, MgO and CaO components in v_5 at 1500 °C. In addition, some differences may be due to complexities in resolving the roles of the three divalent cations (Fe^{2+}, Mg^{2+}, and Ca^{2+}), which sometimes behave similarly (in v_3) and

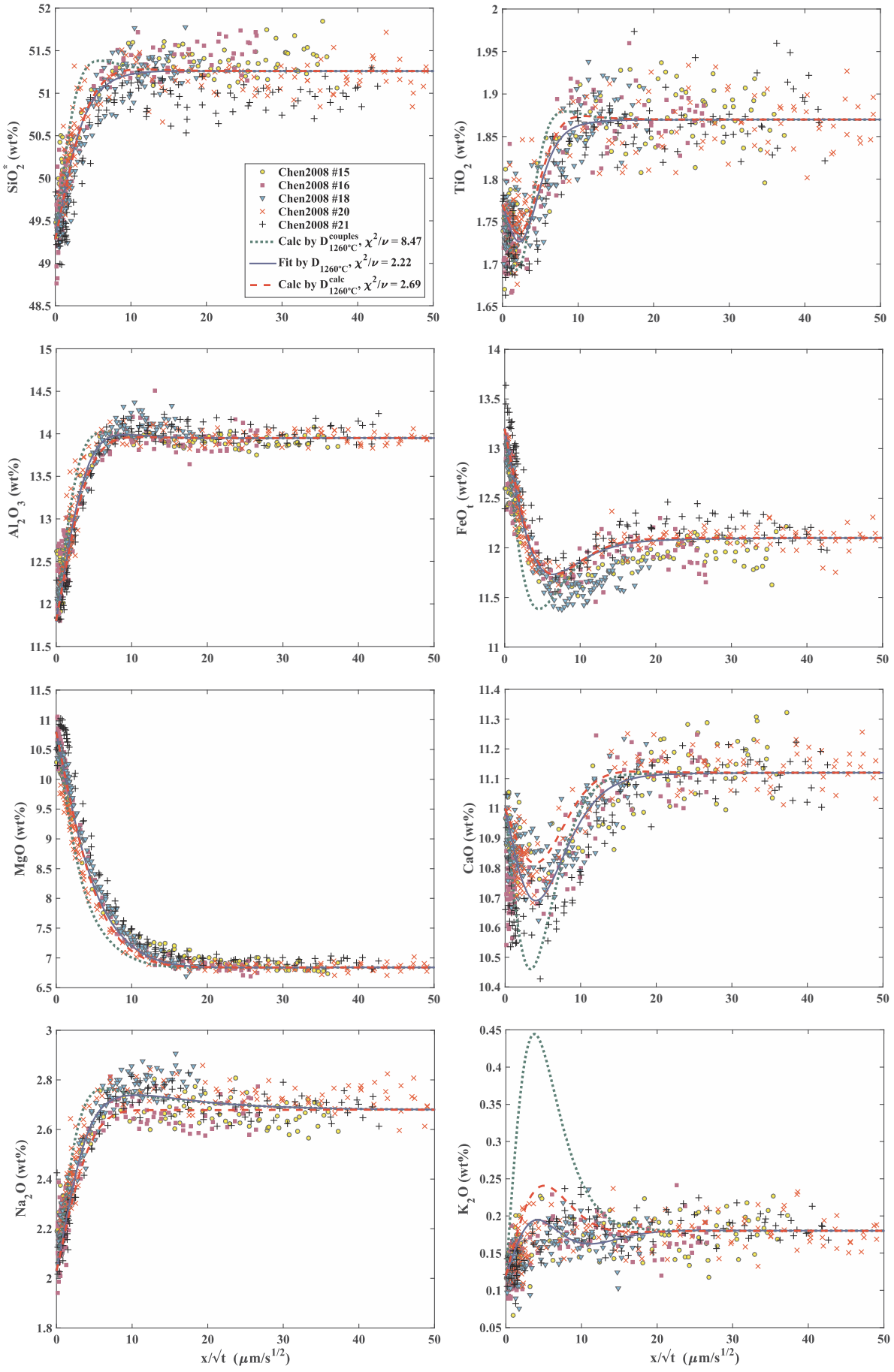

(caption on next page)

Fig. 4. Predicted and fit diffusion profiles for olivine dissolution in basaltic melts at ~1270 °C (Chen and Zhang, 2008). The short-dashed green curves are predicted profiles using $D_{1260°C}^{couples}$ (Table 4). The solid blue curves are fit profiles for obtaining $D_{1260°C}$ (Table 6). The long-dashed red curves are predicted profiles using the calculated diffusion matrix by Eq. (4) and Table 8. χ^2/ν (MSWD) is calculated and shown for each type of predictions and fit. (For interpretation of the references to color in this figure legend, the reader is referred to the web version of this article.)

sometimes differently (v_4 and v_5). The presence of minor amount of Fe^{3+} may also introduce complexity. Note again that K_2O is not a major component in any eigenvector (in eigenvectors including all 8 components, K_2O component is much smaller than 0.5 in any eigenvector).

4.2. Combined fitting of diffusion couple and mineral dissolution experiments at 1260 °C

The extracted diffusion matrices $D_{1260°C}^{couples}$ and $D_{1500°C}^{couples}$ are applied to predict diffusion profiles during olivine, diopside and anorthite dissolution at ~1260 and ~1500 °C (Chen and Zhang, 2008, 2009; Yu et al., 2016) using Eq. (A14) in Appendix A2 of Guo and Zhang (2016). The interface melt composition was estimated by extrapolation from the measured concentration profiles. Even though in theory the interface melt composition can be calculated from the diffusion matrix and chemical potential relations between mineral and melt (Guo and Zhang, 2016), the thermodynamics of basaltic melts is not accurately known for such calculations. The dissolution rate was determined by Eq. (A20) in Appendix A2 of Guo and Zhang (2016), where only the interface-melt concentration of the best-resolved component was used. The predicted results are shown by green short-dash curves in Figs. 4–6. Experimental data for mineral dissolution with similar temperatures and same pressures are plotted together against $x/\sqrt{t}$, and different experiments are indicated by different symbols. The predicted diffusion profiles (short dashed green curve) using $D_{1260°C}^{couples}$ do not match experimental data well, with large MSWD value of 8.5 (Fig. 4), 6.9 (Fig. 5), and 3.1 (Fig. 6) (a high-quality fit has an MSWD value of about 1). For example, the K_2O diffusion profiles are not predicted in all mineral dissolution experiments even though when designing the experiments we increased K_2O concentration in the base composition so as to better constrain the diffusion behavior of K_2O. The reason for the disagreement is not clear, but might be related to the fact that K_2O is not a dominant component in any eigenvectors, making it intrinsically more difficult to model K_2O diffusion behavior during multicomponent diffusion in basalt. There are also other significant mismatches. The disagreement between prediction and experimental data is somewhat disappointing, likely reflecting an inaccurate diffusion matrix, especially due to errors in the eigenvectors (Tables 4 and 5). On the other hand, the imperfect prediction potentially means that including dissolution experiments in fitting the diffusion matrices may significantly improve the accuracy and reliability of the diffusion matrices, as pointed out in Guo and Zhang (2018). Below, we combine mineral dissolution data in the literature with diffusion couple data in this work to fit the diffusion matrix at 1260 °C as in Guo and Zhang (2018).

The diffusion matrix $D_{1260°C}$, with corresponding eigenvalues and eigenvectors, obtained by using both diffusion couple and 3 mineral dissolution experiments, at ~1260 °C is shown in Table 6. The dissolution experiments were run at slightly higher temperatures (1270 and 1280 °C). The solid blue curves in Fig. 2 and Figs. 4–6 are the fit curves for BS5&6C, olivine dissolution, diopside dissolution and anorthite dissolution at ~1260 °C. All the fits by $D_{1260°C}$ for 9 diffusion couple experiments are shown as solid blue curves in Figs. S7–S15 in the Supplementary file. It can be seen from those figures that diffusion profiles in both diffusion couple and mineral dissolution experiments are well reproduced by this diffusion matrix $D_{1260°C}$. The goodness of the fit for diffusion couple experiments is slightly compromised compared to fitting just the diffusion couple experiments, but the fits for 3 mineral dissolution experiments are good to excellent with $\chi^2 = 2.2$, 0.8 and 1.3 respectively. Eigenvectors of $D_{1260°C}$ are similar to those of $D_{1260°C}^{couples}$, but with the following significant differences: v_2 of $D_{1260°C}$ is largely due to Si−Al exchange whereas v_2 of $D_{1260°C}^{couples}$ is largely due to the exchange between Al and other components. For prediction of multicomponent diffusion in basaltic melts at 1260 °C, $D_{1260°C}$ is preferred over $D_{1260°C}^{couples}$ since $D_{1260°C}$ is constrained by more data and can fit diffusion profiles of both diffusion couple and mineral dissolution experiments.

Compared to the data of mineral dissolution experiments at ~1260 °C, concentration profiles in mineral dissolution experiments at ~1500 °C (Chen and Zhang, 2008, 2009; Yu et al., 2016) have larger concentration variations. For example, Al_2O_3 concentration varies from ~13.5 wt% to ~33 wt% during anorthite dissolution, and MgO concentration varies from 7 wt% to ~20 wt% during olivine dissolution. Such large concentration variations would lead to significant variations of the diffusion matrix at a single temperature, and our trial fits show that mineral dissolution data are not well reproduced even though fits are satisfactory with diffusion couple data (Figs. 3, S16–S24). Hence, we decided not to pursue combined fits at 1500 °C.

4.3. Diffusion exchange mechanisms in basaltic melts

On the basis of eigenvectors, diffusion exchange mechanisms in basaltic melts at different temperatures are summarized in Table 7, where data at 1260 °C are from the combined fit (Table 6) of this study, data at 1350 °C are from Guo and Zhang (2018), and data at 1500 °C are from Table 5 of this study. It can be seen that there are similarities in eigenvectors and hence diffusion exchange mechanisms at different temperatures: The largest eigenvalue (v_7) always corresponds to the exchange of Na_2O (and possibly very minor K_2O) with all other components for all 3 temperatures. The third smallest eigenvalue (v_3) corresponds to exchange between divalent oxides and other oxides. The eigenvector corresponding to the exchange of FeO + K_2O with other components is also common at all three temperatures. The two smallest eigenvalues correspond to either SiO_2 exchange with all nonalkalis or SiO_2 exchange with mostly Al_2O_3, or Al_2O_3 exchange with most others. However, the exchange mechanism corresponding to the smallest eigenvalue may vary, probably due to the similar eigenvalues, leading to near-degeneracy (more clearly defined below) with a multiplicity of 2. The other two eigenvectors are more variable at the three temperatures, which might also be related to near-degeneracy. For example, at 1260 °C, three eigenvalues are similar: 19.3, 23.8 and 26.6. The near degeneracy may be partially attributed to the largely similar roles of the three divalent cations (Fe^{2+}, Mg^{2+} and Ca^{2+}) in diffusion, but the roles of Fe^{2+}, Mg^{2+} and Ca^{2+} may also vary slightly as temperature changes and hence melt structure changes.

The near degeneracy of eigenvalues (or nearly degenerate eigenvalues) is not a clearly defined concept even though mathematical degeneracy is well defined. In the case of mathematical degeneracy, different eigenvectors correspond to exactly the same eigenvalue, and eigenvectors are not uniquely defined, because any linear combination

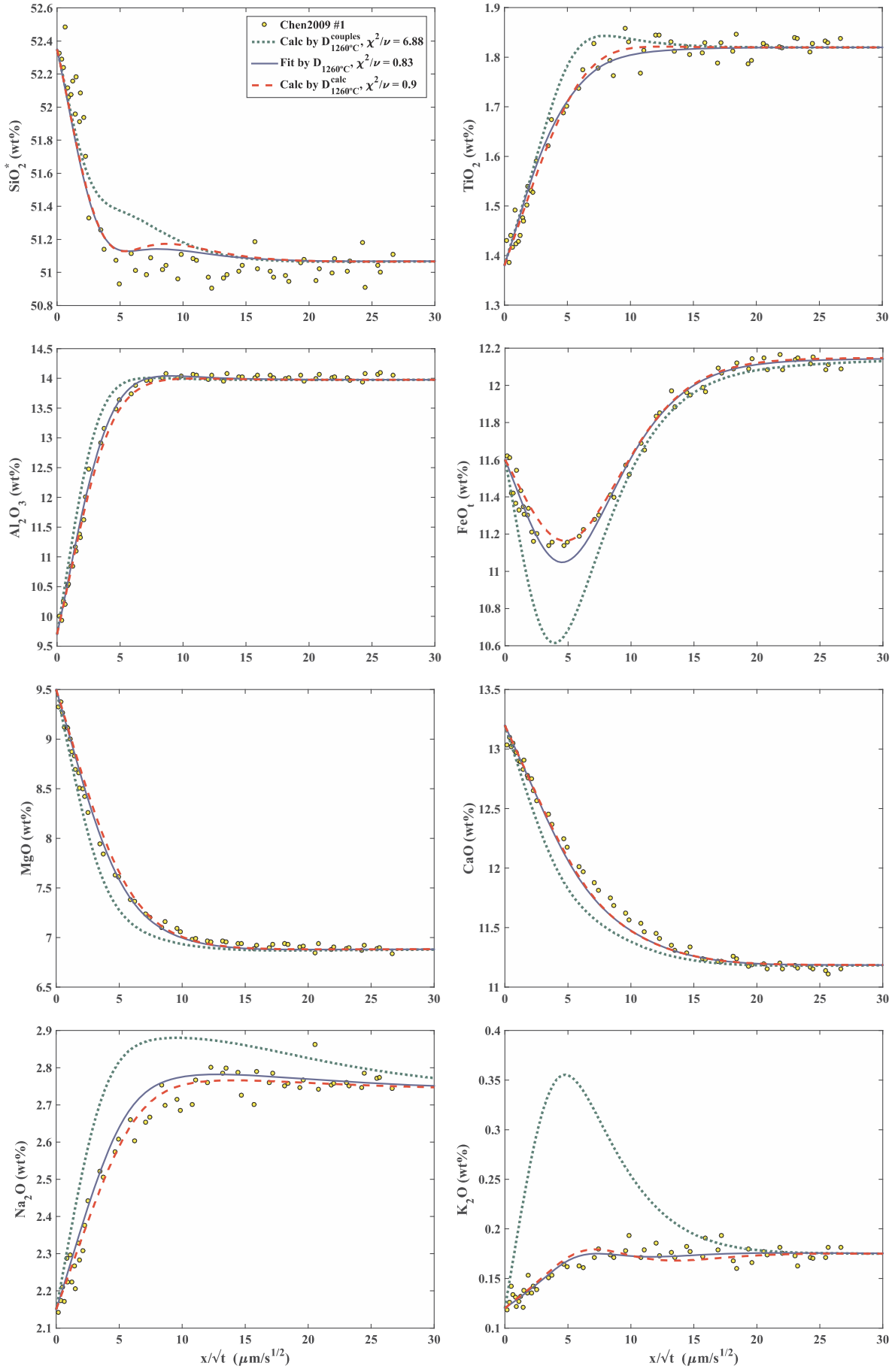

(caption on next page)

Fig. 5. Predicted and fit diffusion profiles for diopside dissolution in basaltic melts at ~1270 °C (Chen and Zhang, 2009). The short-dashed green curves are predicted profiles using $D_{1260°C}^{couples}$ (Table 4). The solid blue curves are fit profiles for obtaining $D_{1260°C}$ (Table 6). The long-dashed red curves are predicted profiles using the calculated diffusion matrix by Eq. (4) and Table 8. χ^2/ν (MSWD) is calculated and shown for each type of predictions and fit. (For interpretation of the references to color in this figure legend, the reader is referred to the web version of this article.)

of two eigenvectors is still an eigenvector. The quantitative criterion of near degeneracy is likely dependent on experimental and analytical data quality. We temporarily define near degeneracy to be two eigenvalues differing by 33% (smaller value divided by the larger value is between 2/3 and 1, or $|\Delta \ln\lambda| \leq 0.4$) for diffusion data extracted from electron microprobe data, because this relative error is about the precision on experimentally determined diffusivity in silicate melts based on electron microprobe data (e.g., Chen and Zhang, 2008, 2009; Zhang et al., 2010) even though the fitting error on individual diffusivity value is often smaller than 10%. Using this criterion, for $D_{1260°C}$, λ_4, λ_5 and λ_6 are nearly triply degenerate; for $D_{1350°C}$ in Guo and Zhang (2018) and $D_{1500°C}^{couples}$ in this work, the following pairs: λ_1 and λ_2, λ_4 and λ_5, and λ_5 and λ_6, are nearly degenerate. In case of near degeneracy, more constraints are necessary to constrain the eigenvectors. These issues will need to be addressed by future research (see Section 5.2).

4.4. Temperature dependence of the D matrix and prediction of diffusion profiles during mineral dissolution

Previous authors have inferred from experimental data in ternary and quaternary systems that the eigenvectors do not vary much but the eigenvalues depend on temperature according to the Arrhenius equation (e.g., Varshneya and Cooper, 1972; Sugawara et al., 1977; Oishi et al., 1982; Chakraborty et al., 1995b; Mungall et al., 1998; Liang and Davis, 2002; Liang, 2010; Pablo et al., 2017; Claireaux et al., 2019). Extracted diffusion matrices and eigenvectors from our experimental data as well as the data in Guo and Zhang (2018) in the eight-component basalt system show indication of such behavior, but are not accurate enough to verify that the eigenvectors are indeed invariant with temperature. Even though our data do not permit an accurate treatment on the temperature dependence of the diffusion matrix in basalt yet, we nonetheless make an attempt to approximate the temperature dependence of the diffusion matrix in basalt by assuming the eigenvector matrix is constant and eigenvalues depends on temperature. *We realize this attempt is a trial attempt for such a complicated system and would like to emphasize that more work is necessary to improve the diffusion matrix, eigenvectors and eigenvalues as a function of temperature.*

The constant eigenvectors are estimated by taking the weighted average of eigenvectors at 3 different temperatures with minor adjustments to improve fits. The weights for eigenvectors are chosen as the inverse exponential of reduced chi-squares in fitting (Edwards, 1972). Note that the sequence and signs of eigenvectors are not fixed, and therefore some eigenvectors need to be multiplied by −1 before taking the average. The estimated invariant eigenvectors, denoted as *P* matrix, are shown in Table 8.

Eigenvalues at each temperature were re-calculated by re-fitting diffusion profiles of both diffusion couple and mineral dissolution experiments by fixing eigenvectors as the invariant eigenvectors *P*. The obtained eigenvalues are plotted in Fig. 7, and each eigenvalue is well fit by Arrhenius relation $\lambda = \lambda_0 \cdot e^{-E/(RT)}$, where λ is in $\mu m^2/s$, *E* is activation energy in kJ/mol and *T* is temperature in K. The fit temperature dependence of the eigenvalue matrix is shown in Table 8, with the largest activation energy of ~170 kJ/mol for λ_1 to λ_3 and the smallest activation energy of 90 kJ/mol for the exchange of Na_2O with all other components (λ_7). The activation energies for λ_1 to λ_3 are similar to that for self diffusion of SiO_2 in a basaltic melt at 1 GPa (e.g., Lesher et al., 1996). The activation energy for λ_7 is similar to that for tracer diffusion of Li_2O, Na_2O and Cu_2O (Zhang et al., 2010; Ni and Zhang, 2016; Ni et al., 2017). By examining Fig. 7, λ_1 and λ_2 are nearly degenerate (differing by < 0.4 natural logarithm units), and λ_4, λ_5 and λ_6 are nearly triply degenerate. Note that when λ values are not nearly degenerate (λ_3 and λ_7), the corresponding eigenvectors (v_3 and v_7) are very consistent at all three temperatures.

To predict multicomponent diffusion in basalt, the diffusion matrix at a given temperature *T* is estimated using the following relation:

$$[D] = [P]\cdot[\lambda(T)]\cdot[P^{-1}], \quad (4)$$

where [*D*] is diffusion matrix in $\mu m^2/s$ (10^{-12} m^2/s), [*P*] is a matrix of the invariant eigenvectors (Table 8) and [$\lambda(T)$] is a diagonal matrix of eigenvalues with Arrhenius relation in Table 8.

To test the robustness of [*P*] and [λ] matrices in Eq. (4), diffusion matrices at 1260 and 1500 °C are calculated from Eq. (4), labeled as $D_{1260°C}^{calc}$ and $D_{1500°C}^{calc}$, and used to predict diffusion profiles in diffusion couple experiments at ~1260 and ~1500 °C, and olivine, diopside and anorthite dissolution experiments in basaltic melts at ~1260 °C (Chen and Zhang, 2008, 2009; Yu et al., 2016). The predicted diffusion profiles are shown by long-dashed red curves in Figs. 2–6, and in Supplementary Figs. S7–S24. The quality of the predictions is similar to that of fitted curves.

Using Eq. (4), the diffusion matrix at 1400 °C is calculated, and diffusion profiles during olivine, diopside and anorthite dissolution at ~1400 °C (Chen and Zhang, 2008, 2009; Yu et al., 2016) are predicted and shown in Figs. 8–10 by long-dashed red curves. For olivine and diopside dissolution in JDF basaltic melt, K_2O diffusion profile is not well predicted in both cases, which might be related to the observation that K_2O is not a dominant component in any eigenvector. For the other profiles, the predicted profiles are often slightly shorter than the experimental profiles, but the shapes are well predicted. Due to the convoluted nature of eigenvectors and eigenvalues, it is not clear whether or not the calculated eigenvalues are too small at this temperature (e.g., the predicted oxide diffusion profiles during anorthite dissolution in Fig. 10 match data well). The prediction for major oxide diffusion during olivine dissolution is better than that during diopside dissolution. For anorthite dissolution in JDF basaltic melt, the predicted diffusion profiles match experimental data well in both diffusion distance and profile shapes. The overall assessment is that the prediction shows preliminary success although improvement is still needed.

5. Further discussion

5.1. Comparison with previous studies

Diffusion matrices reported in literature are mostly for simpler systems, and therefore no direct comparison can be made. The only exception is the 7 × 7 diffusion matrix at 1350 °C for the same basalt system reported by Guo and Zhang (2018), which has been incorporated already in Table 8. Nonetheless, the 7 × 7 diffusion matrices in the 8-component system of this study, such as the diffusion matrix in Table 3

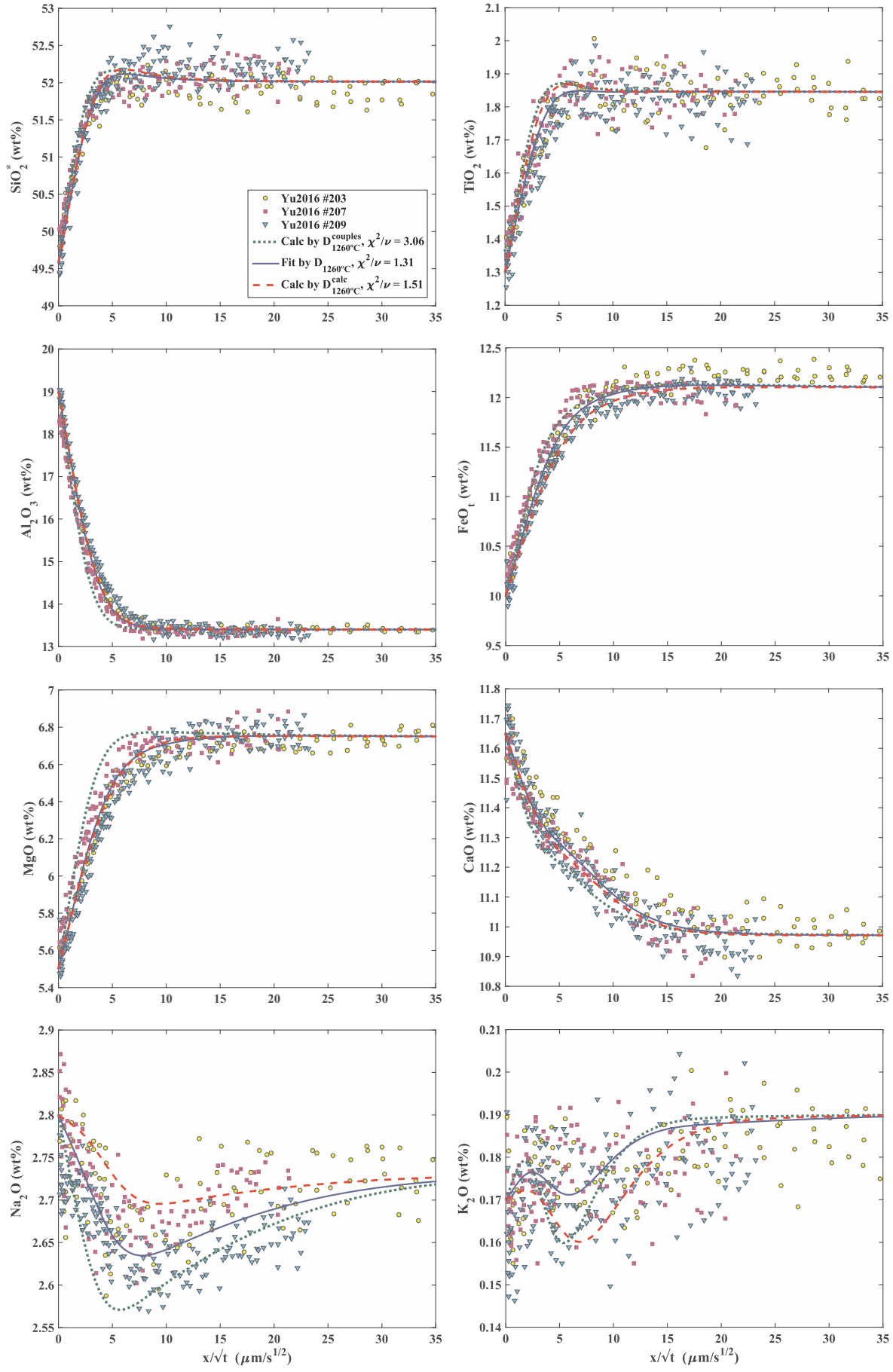

(caption on next page)

Fig. 6. Predicted and fit diffusion profiles for anorthite dissolution in basaltic melts at ~1280 °C (Yu et al., 2016). The short-dashed green curves are predicted profiles using $D_{1260^{\circ}C}^{couples}$ (Table 4). The solid blue curves are fit profiles for obtaining $D_{1260^{\circ}C}$ (Table 6). The long-dashed red curves are predicted profiles using the calculated diffusion matrix by Eq. (4) and Table 8. χ^2/ν (MSWD) is calculated and shown for each type of predictions and fit. (For interpretation of the references to color in this figure legend, the reader is referred to the web version of this article.)

for 1260 °C, the diffusion matrix in Table 5 for 1500 °C and the diffusion matrix calculated at any temperature from Eq. (4), can be compared indirectly with diffusion matrices in literature for simpler system, by retaining rows and columns of the common components. For example, Guo and Zhang (2016) reported a 6 × 6 diffusion matrix for 7-component SiO_2–TiO_2–Al_2O_3–FeO–MgO–CaO–Na_2O–K_2O system at 1500 °C and 1 GPa. There is not much similarity between this matrix and the matrix generated by crossing out the FeO row and FeO column in diffusion matrix in Table 5 or Table 7. One explanation is that the absence of FeO versus the presence of FeO at 10–13 wt% has a significant effect on the diffusion matrix, especially on the eigenvalues. Because the diffusion matrix convolutes the effect of eigenvalues and eigenvectors, direct comparison of the diffusion matrices may be less illuminating than the comparison of diffusion eigenvectors.

When comparing the eigenvectors of different diffusion matrices, it is shown that the slowest eigenvector mostly corresponds to the exchange of SiO_2 with Al_2O_3 in simple systems (Sugawara et al., 1977; Oishi et al., 1982; Chakraborty et al., 1995b; Kress and Ghiorso, 1995; Liang et al., 1996; Mungall et al., 1998; Richter et al., 1998; Liang and Davis, 2002; Liang, 2010; Guo and Zhang, 2016, 2018; Pablo et al., 2017) and the fastest eigenvector is due to the exchange of Na_2O with other components in Na_2O-bearing systems (Watkins et al., 2014; Claireaux et al., 2016, 2019; Guo and Zhang, 2016), consistent with our results. Even though the diffusion matrix in the FeO-free haplobasalt is not very similar to that in the FeO-bearing basalt by crossing out the FeO row and column, the dominant exchange mechanisms (eigenvectors) reported by Guo and Zhang (2016) for the 7-component system are very consistent with those in Table 6 if FeO is ignored. In general, there is similarity in diffusion eigenvectors in different systems, although systems with more components show more exchange mechanisms. However, inconsistency also exists. For example, Claireaux et al. (2016, 2019) found that the slowest diffusion eigenvector is predominantly due to the exchange between Al_2O_3 and CaO, rather than between SiO_2 and Al_2O_3 in a 4-component SiO_2-Al_2O_3-CaO-Na_2O system. Kress and Ghiorso (1995) obtained the slowest diffusion eigenvector being mainly due to the exchange of SiO_2 with FeO + CaO at 1200 °C and the exchange between Al_2O_3 and MgO at 1300 °C in a 6-component SiO_2–TiO_2–Al_2O_3–FeO–MgO–CaO system intended to model Columbia River basalts. The inconsistencies are not readily explained, but uncertainty in diffusion matrix calculation and difference in compositions are possible factors.

5.2. Future improvements of the [D] matrices

Although major efforts and progress were made, improvement of the diffusion matrix in basalt is still needed to be able to predict temperature dependence of *D* matrix and apply it to various geologic applications. This work and the work of Guo and Zhang (2016, 2018) point to some difficulties, but also future directions and strategies for further improving the accuracy of the multicomponent diffusion matrix. One inherit difficulty is the small difference between some eigenvalues for the extracted diffusion matrix, referred to as near degeneracy here. Where near degeneracy is the case, more experiments and better designed experiments are necessary to resolve the diffusion eigenvectors. Another difficulty is that the K_2O component does not appear as a dominant component in any diffusion eigenvector, meaning that it is inherently more difficult to accurately constrain its diffusion behavior.

More accuracy and better constraints are needed to further improve the diffusion matrices. One future strategy is to set up diffusion couples with major concentration gradients in non-SiO_2 components. The issue with using SiO_2 as one of the major concentration gradients is that the analytical error for SiO_2 is larger than for other oxides, leading to more scattered SiO_2 concentration profiles (e.g., comparing SiO_2 and FeO concentration profiles in Fig. 2, and SiO_2 profiles with other profiles in Figs. S1–S6), leading to less precision on the extracted *D* matrix. This is accompanied by the large effect of SiO_2 concentration on diffusion coefficients (e.g., SiO_2 diffusivity varies by a factor of 2 at 1300 °C when SiO_2 concentration varies by 4.3 wt%, Yu et al., 2019), meaning that SiO_2 concentration cannot be varied much more to improve data precision if we want to avoid handling the complexity of variable *D* matrix along concentration profiles. On the other hand, if we use FeO-Na_2O or CaO-Na_2O couples (meaning major and complementary concentration gradients are in FeO and Na_2O or in CaO and Na_2O), the oxide concentrations have smaller analytical errors, resulting in less scattered concentration profiles and hence, at least in theory, a better resolved *D* matrix.

The second future strategy is to specifically constrain the components that show large errors in the eigenvectors. For example, at 1260 °C, the Al_2O_3, FeO, CaO and Na_2O components show larger errors in the eigenvectors (Tables 5 and 6). Therefore, new experiments using Al_2O_3–FeO, FeO–CaO, FeO-Na_2O and CaO-Na_2O couples would likely improve the accuracy of the *D* matrix.

The third future strategy is to slightly increase the initial concentration contrasts. In Guo and Zhang (2016, 2018) and this work, the concentration contrast between the two halves is about 3 wt%. By increasing the contrast to 4 wt% or 5 wt%, the analytical uncertainty would be a smaller fraction of the concentration contrast, leading to better data and hence better constrained *D* matrix. Because Al_2O_3 has a similarly large effect on diffusivity as SiO_2 (Yu et al., 2019), large concentration contrast in Al_2O_3 should also be avoided.

5.3. An application to magma mixing

Magma mixing plays an important role during igneous rock evolution and formation of ore deposits. In the literature, magma mixing is often assumed to be bulk mixing, resulting in linear correlation between elemental concentrations and hyperbola between ratios (Langmuir et al., 1978). However, at the contact of the two magmas, especially if they are partially crystallized, there will be a diffusion zone with a diffusion distance of about 1 m per thousand years. Without the full multicomponent diffusion matrix, it is impossible to explore the intricate compositional variations produced by magma mixing, and some of these variations may affect the formation of ore deposits. For example, uphill diffusion may produce high concentration of some oxide in part of the mixing zone, and low concentration in another part of the mixing zone, which may lead to unexpected formation of some minerals. Here we examine an example of magma mixing in the genesis of platinum-group-elements (PGE) mineralization in the Bushveld Complex, South Africa (Li et al., 2001; Cawthorn, 2002).

Li et al. (2001) and Cawthorn (2002) discussed the mixing between

Table 6
Diffusion matrix $D_{1260°C}$ (μm²/s), obtained by fitting the 9 diffusion couple experiments and 3 mineral dissolution experiments at ~1260 °C, and eigenvalues (μm²/s) and eigenvectors.

$D_{1260°C}$	TiO_2	Al_2O_3	FeO	MgO	CaO	Na_2O	K_2O
TiO_2	2.41(7)	–0.15(5)	–0.85(16)	–0.48(20)	–0.93(27)	–2.40(86)	–1.76(33)
Al_2O_3	–0.25(23)	3.24(11)	–3.87(39)	–0.53(49)	–1.93(63)	–10.6(24)	–6.77(78)
FeO	–7.28(71)	–1.73(34)	6.05(63)	–30.8(9)	–42.4(11)	–106.2(28)	–43.0(13)
MgO	–2.09(35)	–0.10(16)	–6.27(34)	9.11(49)	–14.6(6)	–34.4(19)	–13.3(8)
CaO	–2.59(27)	–3.07(13)	–8.40(30)	–9.66(39)	10.4(5)	–26.6(15)	–0.44(66)
Na_2O	10.2(11)	4.36(43)	20.0(6)	32.6(8)	47.5(11)	185.6(19)	58.9(10)
K_2O	1.85(13)	0.91(5)	2.71(13)	1.85(17)	5.05(23)	7.47(66)	25.6(4)
Eigenvalues (from small to large)							
	λ_1	λ_2	λ_3	λ_4	λ_5	λ_6	λ_7
	1.974(50)	3.178(85)	4.65(10)	19.29(60)	23.8(9)	26.65(71)	162.8(19)
Eigenvectors							
	v_1	v_2	v_3	v_4	v_5	v_6	v_7
TiO_2	–0.58(6)	–0.43(10)	–0.16(2)	0.019(10)	–0.024(10)	0.009(15)	–0.009(5)
Al_2O_3	–0.06(7)	*0.77(25)*	–0.59(9)	0.104(32)	–0.16(6)	0.10(11)	–0.043(12)
FeO	–0.57(3)	0.29(3)	0.62(4)	–0.30(17)	*0.87(57)*	*–0.78(104)*	–0.51(7)
MgO	–0.27(2)	0.14(2)	0.33(2)	–0.58(12)	–0.010(62)	–0.095(46)	–0.16(2)
CaO	–0.43(2)	0.31(2)	0.32(1)	0.66(9)	–0.43(21)	0.59(54)	–0.11(2)
Na_2O	0.20(1)	–0.106(8)	–0.16(1)	0.08(9)	–0.033(19)	–0.096(42)	*0.84(16)*
K_2O	0.164	–0.077	–0.091	0.011	0.168	0.089	0.029
Eigenvectors (showing all 8 components)							
	v_1	v_2	v_3	v_4	v_5	v_6	v_7
SiO_2	0.841	–0.669	–0.262	0.346	–0.352	0.178	–0.035
TiO_2	–0.315	–0.319	–0.152	0.018	–0.0232	0.009	–0.009
Al_2O_3	–0.034	0.576	–0.569	0.098	–0.150	0.098	–0.042
FeO	–0.310	0.218	0.594	–0.286	0.814	–0.769	–0.513
MgO	–0.146	0.102	0.319	–0.548	–0.010	–0.094	–0.158
CaO	–0.234	0.227	0.312	0.617	–0.406	0.585	–0.106
Na_2O	0.110	–0.079	–0.154	0.075	–0.031	–0.095	0.835
K_2O	0.089	–0.057	–0.087	–0.320	0.158	0.088	0.029

See footnote of Table 4.

Table 7
Dominant exchange mechanisms for multicomponent diffusion in basaltic melts at 1260, 1350 and 1500 °C based on their eigenvectors (from smallest to largest eigenvalues).

Eigenvalue	Eigenvector	1260 °C ($D_{1260°C}$)	1350 °C ($D_{1350°C}$)	1500 °C ($D_{1500°C}^{couples}$)
λ_1	v_1	SiO_2 – (all nonalkalis)	SiO_2 – Al_2O_3	(SiO_2 + Al_2O_3) – (all nonalkalis)
λ_2	v_2	(SiO_2 + TiO_2) – (all nonalkalis)	SiO_2 – (most nonalkalis)	Al_2O_3 – (most others)
λ_3	v_3	(FeO + MgO + CaO) – (all others)	(FeO + MgO + CaO) – (all others)	(FeO + MgO + CaO) – (all others)
λ_4	v_4	(MgO + K_2O + FeO) – (all others)	(FeO + K_2O) – (all others)	(FeO + K_2O) – (all others)
λ_5	v_5	(FeO + K_2O) – (all others)	(FeO + CaO) – (MgO + Al_2O_3)	(FeO + CaO) – (all other)
λ_6	v_6	FeO – (most others)	CaO – (most others)	(CaO + K_2O) – (all others)
λ_7	v_7	Na_2O – (all others)	Na_2O – (all others)	Na_2O – (all others)

Table 8
Temperature dependence of eigenvalues [$\lambda(T)$] and the invariant eigenvectors [P] in temperature range from 1260 to 1500 °C.

Eigenvalues ($\mu m^2/s$)

λ_1	λ_2	λ_3	λ_4	λ_5	λ_6	λ_7
$e^{13.752-19,636/T}$						
	$e^{14.737-20,912/T}$					
		$e^{14.897-19,987/T}$				
			$e^{12.375-13880T}$			
				$e^{15.063-18,569/T}$		
					$e^{15.083-18,279/T}$	
						$e^{12.180-10,808/T}$

Invariant eigenvectors [P]

	v_1	v_2	v_3	v_4	v_5	v_6	v_7
TiO_2	−0.76	−0.20	−0.18	−0.02	−0.02	−0.02	−0.02
Al_2O_3	−0.18	0.97	−0.47	−0.15	−0.01	−0.07	−0.10
FeO	−0.51	0.00	0.66	0.86	0.06	−0.41	−0.36
MgO	−0.17	−0.03	0.41	−0.14	−0.71	−0.32	−0.15
CaO	−0.22	0.12	0.33	−0.33	0.70	0.79	−0.08
Na_2O	0.17	−0.04	−0.18	−0.12	−0.04	−0.19	0.91
K_2O	0.13	−0.02	−0.09	0.32	−0.10	0.25	0.06

Note: T is in K, and λ is in $\mu m^2/s$ (10^{-12} m^2/s). The pre-exponential λ_0 value and activation energy E can be calculated, e.g., for $\lambda_1 = e^{13.752-19,636/T}$, as $\lambda_0 = e^{13.752}$ $\mu m^2/s$ and $E = 19636R = 163{,}254$ J/mol = 163 kJ/mol where R is the gas constant.

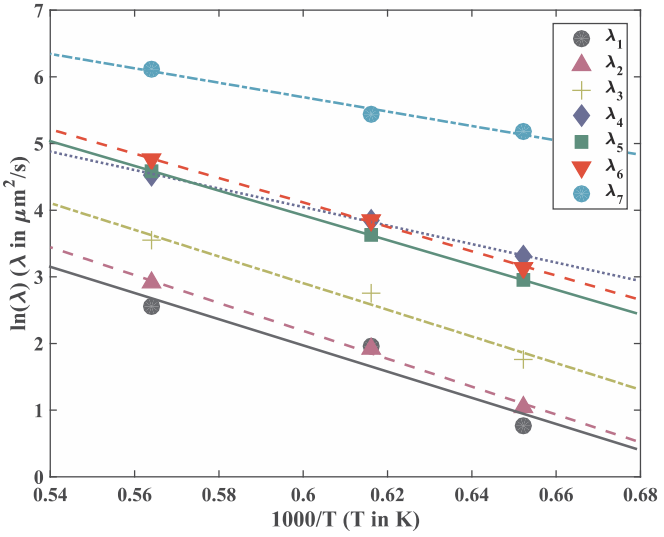

Fig. 7. Logarithm of eigenvalues versus 1000/T in an Arrhenius plot. Eigenvalues were obtained with the fixed invariant eigenvectors [P] in Table 8. The lines are linear fits showing each eigenvalue roughly follows the Arrhenius relation. The fit equations are shown in Table 8.

two melts, a primitive melt and an evolved melt in the Bushveld Complex. They tried to evaluate whether such mixing would lead to sulfide saturation and hence ore formation, meaning whether sulfur concentration in the mixture would exceed sulfide liquid solubility. The equation they used for sulfur solubility is as follows:

$$S = 1431 + 221(FeO - 9) + 5(T - 1200),$$

where S is concentration of sulfur in ppm, FeO is concentration in oxide mol%, and T is temperature in °C. In their modeling, they assumed bulk mixing, leading to linear relations between concentrations. That is, they ignored different diffusion rates and especially cross-diffusion in the multicomponent Bushveld melts. They concluded that magma mixing would not be able to generate reduced FeO concentration and hence reduced sulfur solubility, meaning that mixing of two magmas does not lead to sulfide liquid formation (Cawthorn, 2002; Li, 2002). Here, we examine the consequences of multicomponent diffusion. Li et al. (2001) and Cawthorn (2002) used Zr concentration as an independent parameter to characterize magma mixing. However, because multicomponent diffusion involving Zr has not been quantified, we examine the major oxides only.

The two mixing melts are Melt A and Melt C considered by Li et al. (2001) and Cawthorn (2002). The [D] matrix is calculated from Eq. 4 and Table 8. Melts A and C have higher SiO_2 concentrations than our

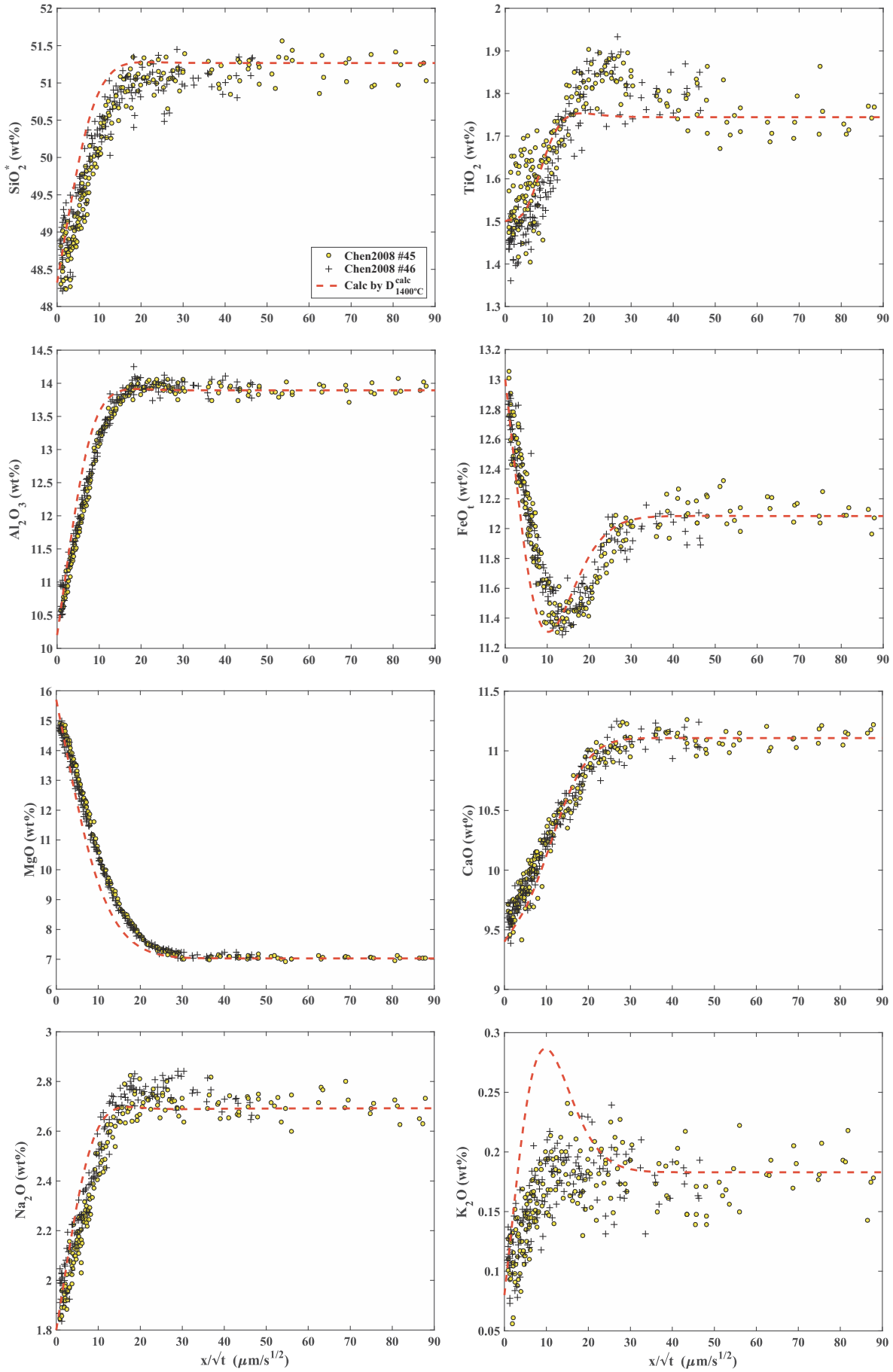

Fig. 8. Predicted diffusion profiles for olivine dissolution in JDF basaltic melts at ~1400 °C (Chen and Zhang, 2008), using the diffusion matrix calculated by Eq. (4) with parameters in Table 8.

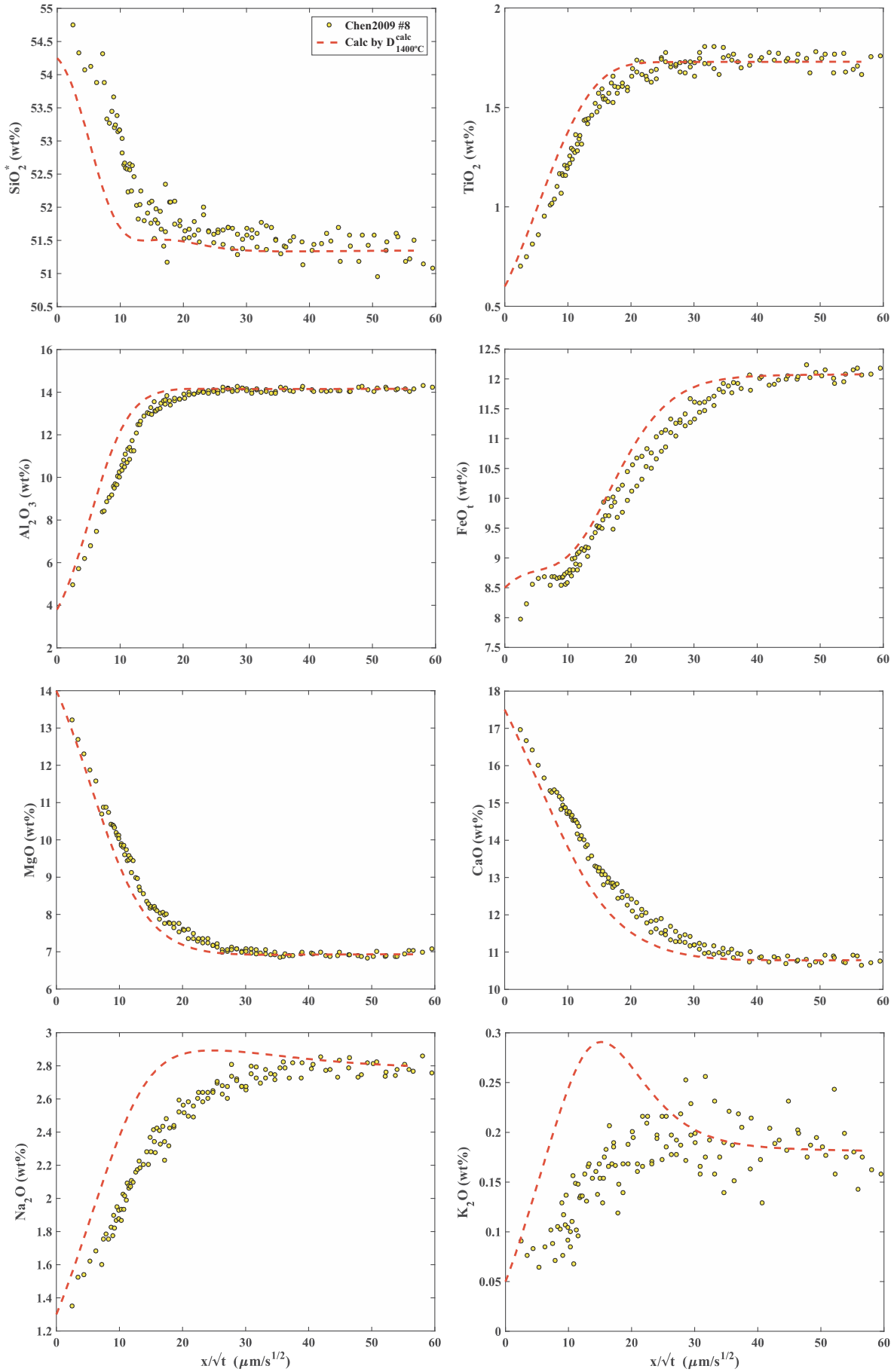

Fig. 9. Predicted diffusion profiles for diopside dissolution in JDF basaltic melts at ~1400 °C (Chen and Zhang, 2009), using the diffusion matrix calculated by Eq. (4) with parameters in Table 8.

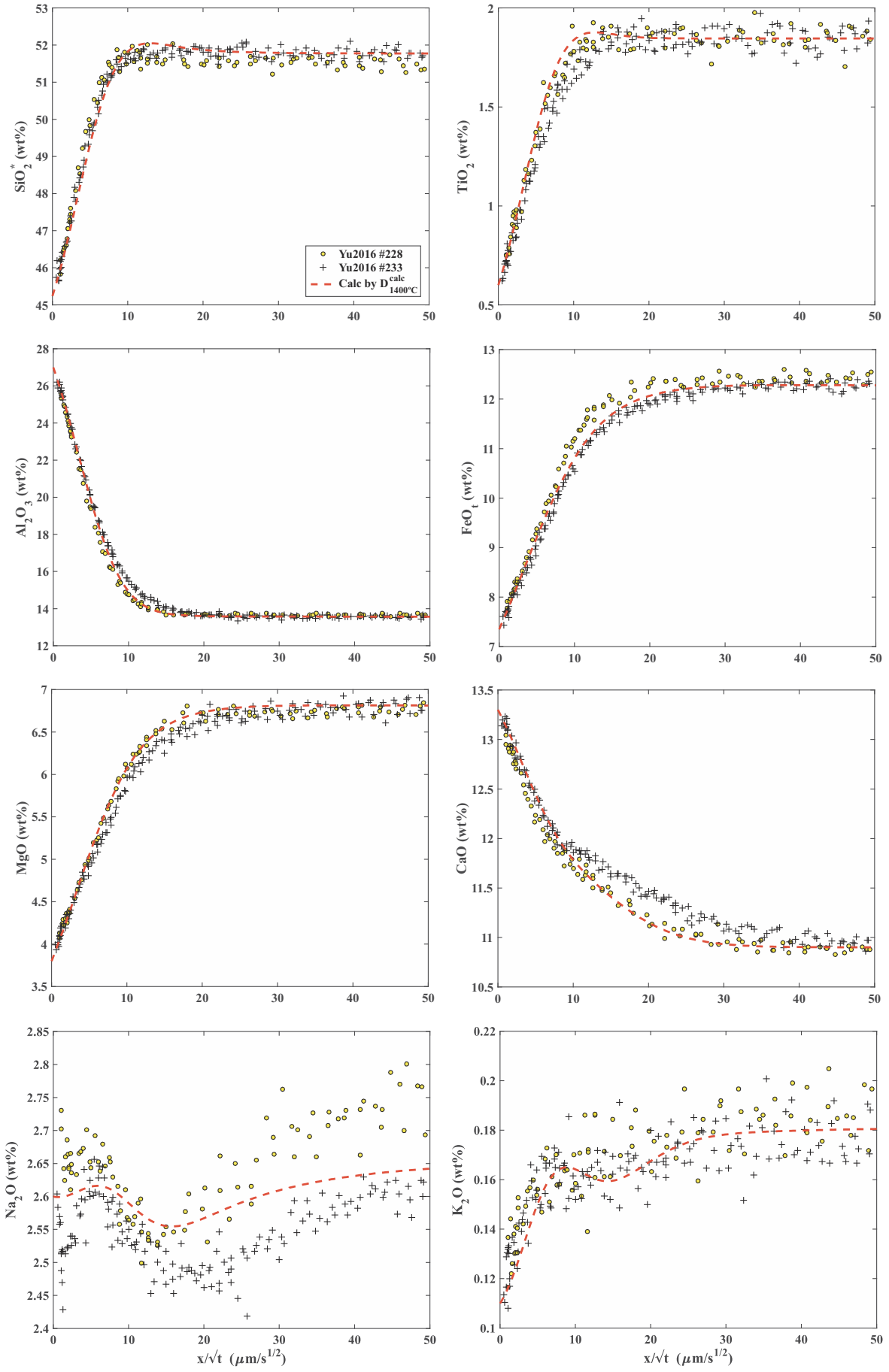

Fig. 10. Predicted diffusion profiles for anorthite dissolution in basaltic melts at ~1400 °C (Yu et al., 2016), using the diffusion matrix calculated by Eq. (4) with parameters in Table 8.

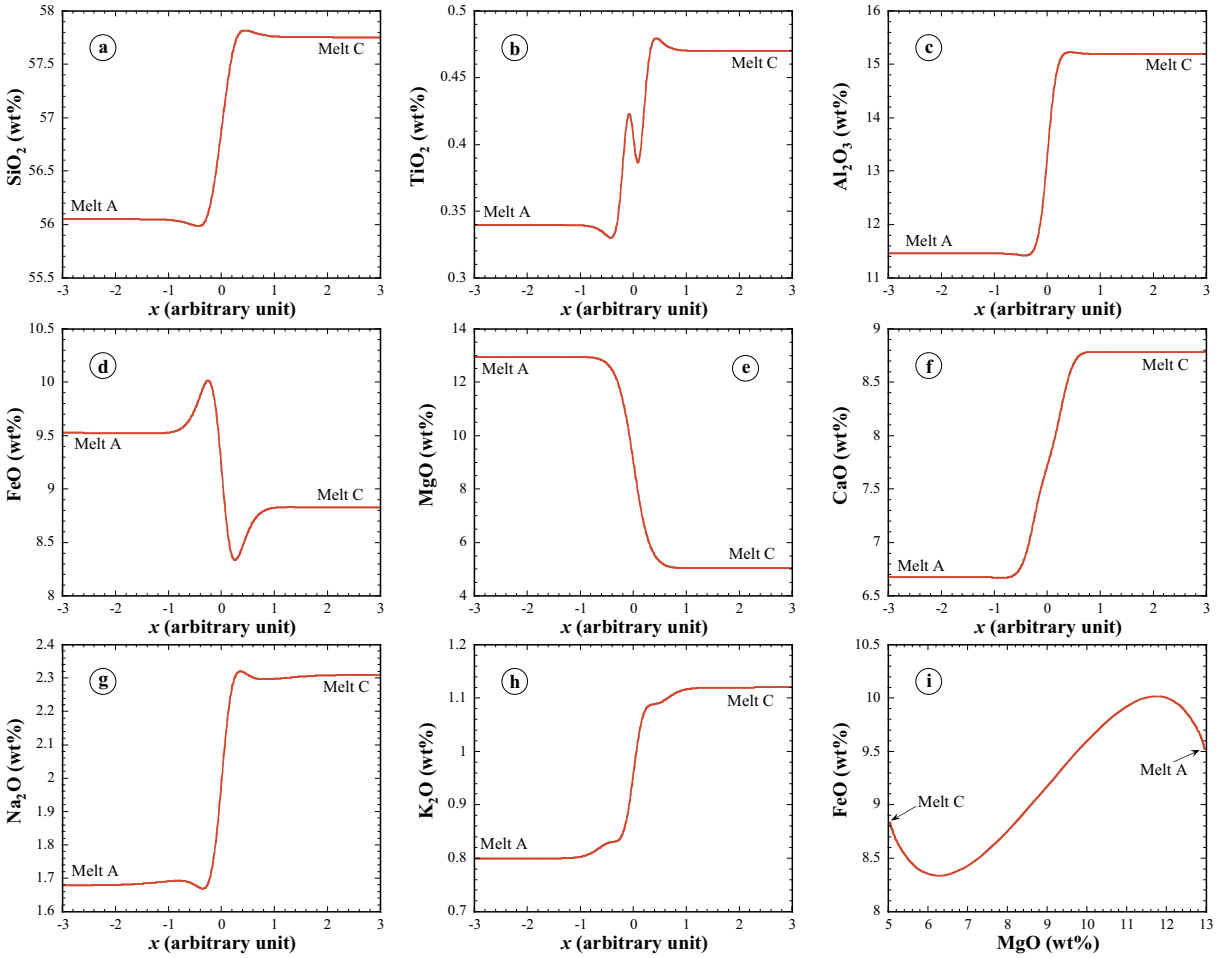

Fig. 11. Calculated concentration profiles due to multicomponent diffusion for magma mixing in the Bushveld Complex. The [*D*] matrix is calculated from Eq. (4) and Table 8 at $T = 1200$ °C. The two initial melts are A and C in Li et al. (2001) and Cawthorn (2002), but Fe_2O_3 (about 0.95 wt%) and FeO are combined into FeO_t.

experimental melts. However, we expect the diffusion eigenvectors in these melts are similar to our results, but the eigenvalues in Melts A and C may be smaller by a factor of 2 to 3 than in our results. Hence, the calculated compositional trends are expected to be reliable. The calculated diffusion profiles of major oxides are shown in Fig. 11. FeO shows clear uphill diffusion (Fig. 11d), which is also often seen in experimental studies (e.g., Zhang et al., 1989; Chen and Zhang, 2008, 2009). The calculated profiles in Fig. 11 show that there are regions with reduced FeO concentration by ~0.5 wt% (~0.4 mol%) than in Melt C (the initial melt with less FeO). In this region with FeO concentration minimum, the sulfur solubility is reduced by 88 ppm, meaning more likelihood of sulfide liquid immiscibility and PGE mineralization. Fig. 11i shows FeO versus MgO relation during magma mixing. This and similar relations may be used to identify effect of multicomponent diffusion during magma mixing.

There is also a significant maximum in FeO concentration (Fig. 11d). Such local high FeO concentration may lead to the formation of Fe—Ti oxide minerals, another possible consequence of multicomponent diffusion effect during magma mixing.

6. Conclusions

Diffusion profiles of 18 successful diffusion couple experiments, nine at 1260 °C and 0.5 GPa and nine at 1500 °C and 1.0 GPa, in 8-component SiO_2–TiO_2–Al_2O_3–FeO–MgO–CaO–Na_2O–K_2O basaltic melts were analyzed by electron microprobe. A diffusion matrix at 1260 °C was obtained by fitting diffusion profiles of both diffusion couple and mineral dissolution experiments simultaneously, while the matrix at 1500 °C was obtained by fitting the data of nine diffusion couple experiments only. All features of diffusion profiles at the same temperature are well reproduced by the respective diffusion matrix. Some eigenvalues of a given diffusion matrix are similar (not identical), a phenomenon we define to be near degeneracy. In such cases, eigenvectors are less well constrained. Diffusion eigenvectors at different temperatures show similarities but are not identical within error. Eigenvalues of diffusion matrices at different temperatures roughly follow the Arrhenius relation. A trial effort was made to obtain the temperature dependence of the diffusion matrix in the basaltic melts by assuming constant eigenvectors and Arrhenian eigenvalues. This way, the diffusion matrix at 1400 °C was calculated and used to predict experimental diffusion profiles during olivine and anorthite dissolution at ~1400 °C reasonably well. We applied our results to model the simultaneous diffusion of all major oxides in the Bushveld Complex during magma mixing, and found that multicomponent diffusion effects may lead to unexpected sulfide mineralization and/or Fe—Ti oxide mineralization. In addition to mixing of mafic magmas, our results can also be used to model multicomponent diffusion during crystal growth and xenolith digestion in mafic melts.

Declaration of competing interest

The authors declare that they have no known competing financial interests or personal relationships that could have appeared to influence the work reported in this paper.

Acknowledgements

We thank Yan Liang, Mike Topless and three anonymous reviewers for insightful comments. This research was supported by US NSF grant EAR-1524473 and EAR-1829822. The electron microprobe Cameca SX100 used in this study was purchased using US NSF grant EAR-9911352.

Appendix A. Supplementary data

Two supplementary files are provided. One is a pdf file for additional figures associated with this article, and diffusion matrix when a different oxide component (other than SiO_2) is used as the independent component. These matrices are provided for the convenience of readers in their applications. The second supplementary file contains concentration profiles of all 18 diffusion couple experiments. Supplementary data to this article can be found online at https://doi.org/10.1016/j.chemgeo.2020.119700.

References

Cawthorn, R.G., 2002. The role of magma mixing in the genesis of PGE mineralization in the Bushveld Complex: thermodynamic calculations and new interpretations - a discussion. Econ. Geol. 97, 663–667.
Chakraborty, S., Dingwell, D.B., Rubie, D.C., 1995a. Multicomponent diffusion in ternary silicate melts in the system K_2O-Al_2O_3-SiO_2: I. Experimental measurements. Geochim. Cosmochim. Acta 59, 255–264.
Chakraborty, S., Dingwell, D.B., Rubie, D.C., 1995b. Multicomponent diffusion in ternary silicate melts in the system K_2O-Al_2O_3-SiO_2: II. Mechanisms, systematics, and geological applications. Geochim. Cosmochim. Acta 59, 265–277.
Chen, Y., Zhang, Y., 2008. Olivine dissolution in basaltic melt. Geochim. Cosmochim. Acta 72, 4756–4777.
Chen, Y., Zhang, Y., 2009. Clinopyroxene dissolution in basaltic melt. Geochim. Cosmochim. Acta 73, 5730–5747.
Claireaux, C., et al., 2016. Atomic mobility in calcium and sodium aluminosilicate melts at 1200°C. Geochim. Cosmochim. Acta 192, 235–247.
Claireaux, C., et al., 2019. Influence of temperature on multicomponent diffusion in calcium and sodium aluminosilicate melts. J. Non-Cryst. Sol. 505, 170–180.
Clifford, A.A., 1973. Multivariate Error Analysis. Wiley, New York (112 pp).
Cooper, A.R., 1968. The use and limitations of the concept of an effective binary diffusion coefficient for multi-component diffusion. In: Wachman, J.B., Franklin, A.D. (Eds.), Mass Transport in Oxides. Nat. Bur. Stand. Spec. Publ, pp. 79–84.
Dixon, J.E., Stolper, E.M., Delaney, J.R., 1988. Infrared spectroscopic measurements of CO_2 and H_2O in Juan de Fuca Ridge basaltic glasses. Earth Planet. Sci. Lett. 90, 87–104.
Edwards, A.W.F., 1972. Likelihood. Cambridge University Press (300 pp.).
Fletcher, R., 1971. A modified Marquardt subroutine for nonlinear least squares. In: Atomic Energy Research Establishment R6799, Harwell, England, (28 pp).
Guo, C., Zhang, Y., 2016. Multicomponent diffusion in silicate melts: SiO_2-TiO_2-Al_2O_3-MgO-CaO-Na_2O-K_2O system. Geochim. Cosmochim. Acta 195, 126–141.
Guo, C., Zhang, Y., 2018. Multicomponent diffusion in basaltic melts at 1350°C. Geochim. Cosmochim. Acta 228, 190–204.
Hui, H., Zhang, Y., Xu, Z., Behrens, H., 2008. Pressure dependence of the speciation of dissolved water in rhyolitic melts. Geochim. Cosmochim. Acta 72, 3229–3240.
Koyaguchi, T., 1985. Magma mixing in a conduit. J. Volcanol. Geotherm. Res. 25, 365–369.
Koyaguchi, T., 1989. Chemical gradient at diffusive interfaces in magma chambers. Contrib. Mineral. Petrol. 103, 143–152.
Kress, V.C., Ghiorso, M.S., 1993. Multicomponent diffusion in MgO-Al_2O_3-SiO_2 and CaO-MgO-Al_2O_3-SiO_2 melts. Geochim. Cosmochim. Acta 57, 4453–4466.
Kress, V.C., Ghiorso, M.S., 1995. Multicomponent diffusion in basaltic melts. Geochim. Cosmochim. Acta 59, 313–324.
Langmuir, C.H., Vocke, R.D., Hanson, G.N., Hart, S.R., 1978. A general mixing equation with application to Icelandic basalts. Earth Planet. Sci. Lett. 37, 380–392.
Lesher, C.E., Hervig, R.L., Tinker, D., 1996. Self diffusion of network formers (silicon and oxygen) in naturally occurring basaltic liquid. Geochim. Cosmochim. Acta 60, 405–413.
Li, C., 2002. The role of magma mixing in the genesis of PGE mineralization in the Bushveld Complex: thermodynamic calculations and new interpretations - a reply. Econ. Geol. 97, 667.
Li, C., Maier, W.D., de Waal, S.A., 2001. The role of magma mixing in the genesis of PGE mineralization in the Bushveld Complex: thermodynamic calculations and new interpretations. Econ. Geol. 96, 653–662.
Liang, Y., Davis, A.M, 2002. Energetics of multicomponent diffusion in molten CaO-Al2O3-SiO2. Geochim. Cosmochim. Acta 66, 635–646.
Liang, Y., 2010. Multicomponent diffusion in molten silicates: theory, experiments, and geological applications. Rev. Mineral. Geochem. 72, 409–446.
Liang, Y., Richter, F.M., Watson, E.B., 1996. Diffusion in silicate melts, II: multicomponent diffusion in CaO-Al2O3-SiO2 at 1500°C and 1 GPa. Geochim. Cosmochim. Acta 60, 5021–5035.
Macris, C.A., et al., 2018. Seconds after impact: insights into the thermal history of impact ejecta from diffusion between lechateliertite and host glass in tektites and experiments. Geochim. Cosmochim. Acta 241, 69–94.
Mungall, J.E., Romano, C., Dingwell, D.B., 1998. Multicomponent diffusion in the molten system K_2O-Na_2O-Al_2O_3-SiO_2-H_2O. Am. Mineral. 83, 685–699.
Ni, P., Zhang, Y., 2016. Cu diffusion in a basaltic melt. Am. Mineral. 101, 1474–1482.
Ni, P., Zhang, Y., Simon, A., Gagnon, J., 2017. Cu and Fe diffusion in rhyolitic melts during chalcocite “dissolution”: implications for porphyry ore deposits and tektites. Am. Mineral. 102, 1287–1301.
Oishi, Y., Nanba, M., Pask, J.A., 1982. Analysis of liquid-state interdiffusion in the system CaO-Al_2O_3-SiO_2 using multiatomic ion models. J. Am. Ceram. Soc. 65, 247–253.
Oldenburg, C.M., Spera, F.J., Yuen, D.A., Sewell, G., 1989. Dynamic mixing in magma bodies: theory, simulations, and implications. J. Geophys. Res. 94, 9215–9236.
Pablo, H., Schuller, S., Toplis, M.J., Gouillart, E., Mostefaoui, S., Charpetier, T., Roskosz, M., 2017. Multicomponent diffusion in sodium borosilicate glasses. J. Non-Cryst. Sol. 478, 29–40.
Richter, F., Liang, Y., Minarik, W.G., 1998. Multicomponent diffusion and convection in molten MgO-Al_2O_3-SiO_2. Geochim. Cosmochim. Acta 62, 1985–1991.
Sato, H., 1975. Diffusion coronas around quartz xenocrysts in andesite and basalt from Tertiary volcanic region in northeastern Shikoku, Japan. Contrib. Mineral. Petrol. 50, 49–64.
Sugawara, H., Nagata, K., Goto, K.S., 1977. Interdiffusivities matrix of CaO-Al_2O_3-SiO_2 melt at 1723 K to 1823 K. Metall. Trans. A. 8B (December), 605–612.
Trial, A.F., Spera, F.J., 1994. Measuring the multicomponent diffusion matrix: experimental design and data analysis for silicate melts. Geochim. Cosmochim. Acta 58, 3769–3783.
Turner, J.S., 1985. Multicomponent convection. Annu. Rev. Fluid Mech. 17, 11–44.
Varshneya, A.K., Cooper, A.R., 1972. Diffusion in the system K_2O-SrO-SiO_2, III: interdiffusion coefficients. J. Am. Ceram. Soc. 55, 312–317.
Watkins, J.M., Liang, Y., Richter, F., Ryerson, F.J., DePaolo, D.J., 2014. Diffusion of multiisotopic chemical species in molten silicates. Geochim. Cosmochim. Acta 139, 313–326.
Watson, E.B., 1982. Basalt contamination by continental crust: some experiments and models. Contrib. Mineral. Petrol. 80, 73–87.
Yu, Y., Zhang, Y., Chen, Y., Xu, Z., 2016. Kinetics of anorthite dissolution in basaltic melt. Geochim. Cosmochim. Acta 179, 257–274.
Yu, Y., Zhang, Y., Yang, Y., 2019. Kinetics of quartz dissolution in natural silicate melts and dependence of SiO2 diffusivity on melt composition. ACS Earth Space Chem. 3, 599–616.
Zhang, Y., 1993. A modified effective binary diffusion model. J. Geophys. Res. 98, 11901–11920.
Zhang, Y., 2008. Geochemical Kinetics. Princeton University Press, Princeton, NJ (664 pp).
Zhang, Y., Behrens, H., 2000. H_2O diffusion in rhyolitic melts and glasses. Chem. Geol. 169, 243–262.
Zhang, Y., Stolper, E.M., 1991. Water diffusion in basaltic melts. Nature 351, 306–309.
Zhang, Y., Walker, D., Lesher, C.E., 1989. Diffusive crystal dissolution. Contrib. Mineral. Petrol. 102, 492–513.
Zhang, Y., Ni, H., Chen, Y., 2010. Diffusion data in silicate melts. Rev. Mineral. Geochem. 72, 311–408.